

## Motor Flow Instabilities – Part 1

F. Vuillot, G. Casalis

ONERA

BP 72

92322 Châtillon Cedex

FRANCE

<b>Introduction</b>	<b>1</b>
<b>Motor Stability</b>	<b>2</b>
General Overview	2
Acoustic Balance	5
Particular Contributions to the Acoustic Balance	10
Flow Turning Issue	12
Two-Phase Flows	13
Conclusion/Limitations	15
<b>Flow Stability</b>	<b>15</b>
Presentation	15
Intrinsic Non-Linear Nature	17
Model Requirements	17
<b>Stability Theory</b>	<b>19</b>
<b>Dealing with Flow Stability</b>	<b>19</b>
Experimental Evidences	19
Simplified Approaches	22
Full Numerical Approaches	25
Examples	26
<b>Conclusions/Unsettled Issues</b>	<b>33</b>
<b>Acknowledgement</b>	<b>34</b>
<b>References</b>	<b>34</b>

## INTRODUCTION

This paper will be given in two separate talks, a first one presenting the general problem and applications to actual motors and a second talk dealing more specifically with stability theory.

Solid propellant rocket motor instability has been the subject of many research works for more than 40 years and valuable reviews can be found in references [1, 2]. First concerns were to understand the sometimes violent instabilities that occurred during motor firings that could lead to motor failure or destruction. The combustion mechanisms were among the first to be studied since most of the energy released in the motor chamber is due to chemical reactions linked to propellant combustion. Indeed, only a very small fraction of this energy could, if directed to few instability modes, results in abnormal strains that could lead to propellant or case failure and then to motor destruction (see [2]). Instability modes can be of several types and had been classified into volume modes and acoustic modes (see [1]). Only the latter will be considered here since they appeared to be the most unpredictable. In such situations, the instabilities organize themselves around chamber acoustic modes and produce acoustic resonances,

*Paper presented at the RTO/VKI Special Course on “Internal Aerodynamics in Solid Rocket Propulsion”, held in Rhode-Saint-Genèse, Belgium, 27-31 May 2002, and published in RTO-EN-023.*

Report Documentation Page			Form Approved OMB No. 0704-0188		
Public reporting burden for the collection of information is estimated to average 1 hour per response, including the time for reviewing instructions, searching existing data sources, gathering and maintaining the data needed, and completing and reviewing the collection of information. Send comments regarding this burden estimate or any other aspect of this collection of information, including suggestions for reducing this burden, to Washington Headquarters Services, Directorate for Information Operations and Reports, 1215 Jefferson Davis Highway, Suite 1204, Arlington VA 22202-4302. Respondents should be aware that notwithstanding any other provision of law, no person shall be subject to a penalty for failing to comply with a collection of information if it does not display a currently valid OMB control number.					
1. REPORT DATE <b>00 JAN 2004</b>		2. REPORT TYPE <b>N/A</b>		3. DATES COVERED <b>-</b>	
4. TITLE AND SUBTITLE <b>Motor Flow Instabilities Part 1</b>				5a. CONTRACT NUMBER	
				5b. GRANT NUMBER	
				5c. PROGRAM ELEMENT NUMBER	
6. AUTHOR(S)				5d. PROJECT NUMBER	
				5e. TASK NUMBER	
				5f. WORK UNIT NUMBER	
7. PERFORMING ORGANIZATION NAME(S) AND ADDRESS(ES) <b>ONERA BP 72 92322 Châtillon Cedex FRANCE</b>				8. PERFORMING ORGANIZATION REPORT NUMBER	
9. SPONSORING/MONITORING AGENCY NAME(S) AND ADDRESS(ES)				10. SPONSOR/MONITOR'S ACRONYM(S)	
				11. SPONSOR/MONITOR'S REPORT NUMBER(S)	
12. DISTRIBUTION/AVAILABILITY STATEMENT <b>Approved for public release, distribution unlimited</b>					
13. SUPPLEMENTARY NOTES <b>See also ADM001656., The original document contains color images.</b>					
14. ABSTRACT					
15. SUBJECT TERMS					
16. SECURITY CLASSIFICATION OF:			17. LIMITATION OF ABSTRACT <b>UU</b>	18. NUMBER OF PAGES <b>38</b>	19a. NAME OF RESPONSIBLE PERSON
a. REPORT <b>unclassified</b>	b. ABSTRACT <b>unclassified</b>	c. THIS PAGE <b>unclassified</b>			

much like an organ pipe. The fact that motor combustion chamber consists of a closed cavity (except for the nozzle, but we will see that it may be assimilated to an acoustically closed end) favors that interpretation. The so-called acoustic balance methods belong to that vision. Expressions for gains and losses to given chamber acoustic modes are looked for from knowledge of propellant combustion and mean flow organization incorporated into a linearized analysis. The objective is to identify modes that could be linearly unstable, that is to say that would grow to infinite amplitudes from infinitely small perturbations. In that acoustic view and in order to obtain tractable expressions, the flow field had to be idealized and was viewed as a perturbation of acoustic equations. However in the last 20 years it became evident that the complexity of the chamber internal flows could produce flow instabilities that could alone drive the resonance. Interestingly enough, the musical paradigm was shifted to the flute, where the role of air motion is more evident than in an organ pipe (although the physical mechanisms are very much the same). In that process, most of the simplified hypotheses of the acoustic balance approach had to be questioned and the resulting vision was much more general and embraced the entire internal flow (including combustion) and the instabilities were non longer solely combustion instabilities but flow instabilities.

Before we go into the details of that paper, few remarks must be made, relative to time and length scales. Although solid propellant motors have the particularity of having a combustion chamber whose geometry continuously varies with time (due to propellant combustion) analysis of time scales permits to consider a succession of fixed geometries. Indeed the propellant regression rate ( $< 1 \text{ cm/s}$ ) is at least two order of magnitude smaller than flow velocity (few  $\text{m/s}$ ) which is itself at least two order of magnitude smaller than the speed of sound ( $1000 \text{ m/s}$ ) that governs the propagation of acoustic waves. As a result, one can considers that the geometry is fixed during the time one looks at vortices development and displacement into the chamber or the time one looks at the amplification of an acoustic wave during few cycles. Only analysis of long time behaviors or hysteresis phenomenons would require the consideration of propellant surface regression. A similar analysis can be performed for the length scales. Indeed, propellant gaseous combustion occurs in few tens of microns above the propellant surface, while the vortices or acoustic length scales are often close to the  $\text{cm}$  or  $\text{m}$ . Again, one can consider the combustion of gaseous species to be assimilated to the boundary conditions of the instability problem. Only the case of condensed phase combustion (typically aluminum combustion) which has length scale of  $\text{cm}$ , could impact the instability analysis. This will be discussed later on.

Another remark must be made at this stage. A quick view of motor operating pressures (in the range of several  $10^6 \text{ Pa}$ ) and temperatures (from  $2600$  to  $3600 \text{ K}$ ) indicates that measurements inside the motor is a challenging task (not mentioning the vibrations, the presence of combustion products in condensed phase and the difficulty of drilling holes for probe access in a lightweight pressurized vessel). It is thus an evidence that measurements in a production motor is scarce and that only research motors can be equipped with the needed transducers to acquire a satisfactory knowledge of what is going on inside. Most often, investigators must rely on a limited number of pressure transducers, only some of them being rated for the necessary unsteady measurements. To compensate these intrinsic difficulties, researchers have developed several means of simulating rocket motor operating conditions. These rank from cold flow simulators, where air, or nitrogen, is injected through porous surfaces that simulate the motor geometry at chosen time points during the burn and, more recently, to numerical simulations of chamber internal flows, again at chosen time points during the burn. These simulations permit to access to the details of the internal flow which complement the pressure measurements obtained from actual motor firings.

## **MOTOR STABILITY**

### **General Overview**

Motor stability discussion will be limited to the case of acoustic instabilities, where the fluctuating field is organized around the chamber standing acoustic modes. The case of longitudinal modes is the most

documented case and will be used throughout this paper. Extensions to transverse modes (radial or tangential modes), although important, will not be directly addressed nor can it be either easily deduced from the presented materials. The interested reader is let to work out his way in that matter by his own.

Analysis of motor stability relies on the following simple decomposition:  $P(\mathbf{r}, t) = \bar{P}(\mathbf{r}) + p'(\mathbf{r}, t)$ , where overbar indicates mean values, prime indicates fluctuating values,  $\mathbf{r}$  is the position vector and  $t$  is the time variable. This decomposition is general and no assumptions are made at this point.

The figure below presents a schematic of physical processes that take place inside a solid propellant rocket motor.

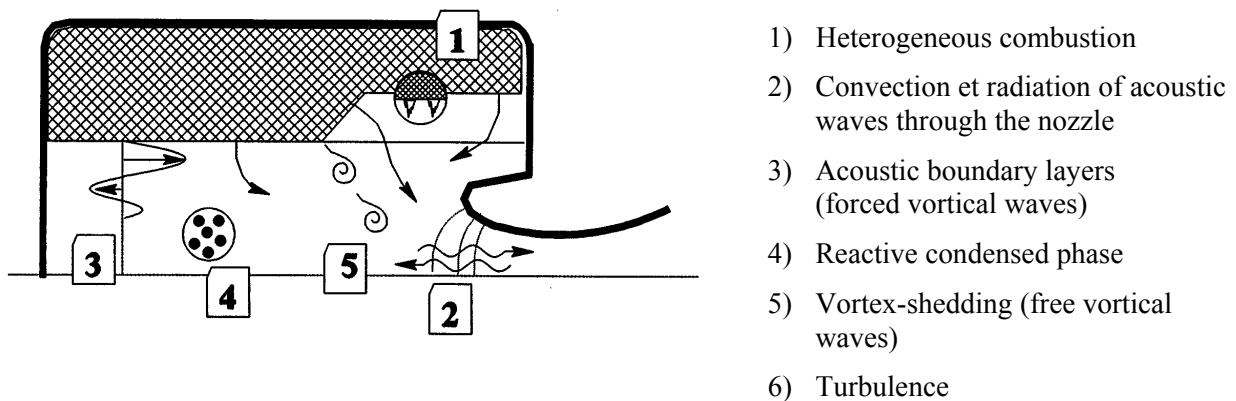


**Figure 1: Physical Phenomenons in a SRM.**

Not all these phenomenons are directly taken care of in usual approaches of motor instabilities. Approximations are common place, due to the lack of knowledge and/or the complexity of the mechanisms. For instance, the heterogeneous nature of the combustion of solid propellant is rarely given a full treatment, most often, it is averaged and treated as an equivalent homogeneous process, such as burning rate laws ( $ap^n$ ) or response functions to fluctuating pressure. Nozzle treatment relies on numerous analyses and is quite satisfactory, at least for the most classical case of longitudinal modes and axial nozzles. Acoustic boundary layers is a particular topic which corresponds to attempts to introduce the vortical nature of the unsteady flow into acoustic treatments. We will see that this question largely overpasses the simple acoustic treatment since the notion of unsteady vorticity fiercely opposes the acoustic point of view. For the present time, it suffices to say that unsteady vortical waves are naturally generated when an acoustic wave sweeps above the burning propellant surface, where the velocity is forced to be perpendicular to the surface (no slip condition). The role of viscosity in that process has been misunderstood (as essential in stating the no-slip condition while this condition can be simply, in an inviscid view, linked to mass and momentum balances at the propellant surface) and finally may appear to be of secondary importance. However, the impact of this process on the acoustic balance is important and the fact that it is not yet fully understood does not diminish its role. Quite often the condensed phase is considered as inert (e.g. alumina droplets) and composed of a limited number of sizes, although it is known that aluminum burns in a complex (and not yet perfectly known) manner, generating a continuum of droplet sizes, from the microns to the tenths of millimeter sizes. This matter constitutes one of the presently active research issues relative to motor stability and will be discussed later on. Vortex-shedding will also be discussed in some details later on, since the research is much more advanced on that subject. Its merit is to introduce the flow field as an actor to its own destabilization. Indeed periodic vortex-shedding can be viewed as a path for energy to be transferred from the mean flow to the fluctuating field. The fact that vortex-shedding can occur at discrete frequencies, some of them being capable of matching acoustic frequencies, differentiates this mechanism from the next one, turbulence, which rather implies a

## Motor Flow Instabilities – Part 1

continuum of frequencies. Although turbulence is also an energy path between the mean flow and the fluctuating field, the lack of distinguished frequencies makes this path much less effective in producing instabilities. Indeed, the gained experience shows that large turbulent levels inhibit motor instabilities which are built on a delicate balance of resonant mechanisms. However, it must not be forgotten that turbulence, when limited to usual levels, is also a very effective seed to local instabilities that can then feed the overall instability mechanisms.

It is useful to consider the equation for a simple oscillator of state variable  $p$ , where dot indicates time derivative,  $\alpha$  the linear damping coefficient,  $\omega$  the angular frequency and  $F(t)$  a forcing function:

$$\ddot{p} + 2\alpha\dot{p} + \omega^2 p = F(t)$$

$$\alpha < 0 \quad \text{unstable}$$

$$\alpha > 0 \quad \text{stable}$$

This apparently linear equation can bear some form of non-linearities that can show up in the form of dependencies of the coefficients on the state variable,  $p$ , such as  $\alpha(p)$  or  $F(p, t)$ . Under the assumption that  $\alpha \ll \omega$ , the solution of the linear homogeneous equation takes the simple form,  $p = p_0 \exp(i\omega t - \alpha t)$ .

The figures below depict particular behaviors:

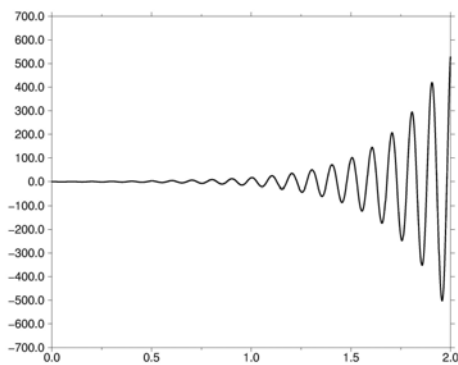


**Figure 2-a: Linearly Unstable.**

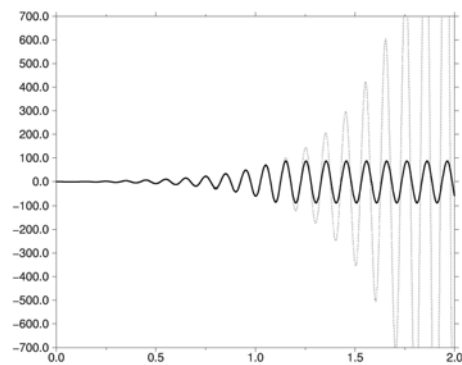


**Figure 2-b: Harmonically Forced Linearly Unstable and Non-Linearly Stable ( $\alpha > 0$  for Large Amplitudes).**

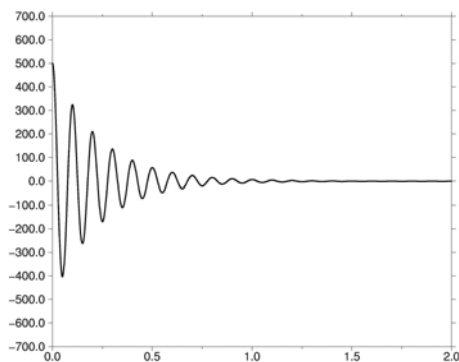


**Figure 2-c: Linearly Stable.**

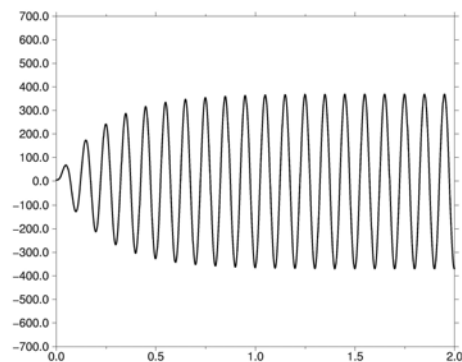


**Figure 2-d: Linearly Stable, Harmonically Forced.**

It can be seen that cases b) and d) lead to limit amplitudes when some harmonic forcing functions are applied. Case d) is of particular interest since it may correspond to actual behaviors observed in large segmented space boosters, which while predicted linearly stable, exhibit limit amplitude cycles. For these cases, it is believed that periodic vortex-shedding could be the forcing function, although this point remains largely open to debate.

## Acoustic Balance

Before recalling the acoustic balance approach, it must be stressed that acoustic balance methods can be viewed as a linear analysis of the stability of chamber acoustic modes, much like the above simple oscillator examples. In the absence of forcing function, an inhomogeneous Helmholtz equation and its boundary conditions are derived from the linearized equations of motion. Inhomogeneities arise from considerations of the mean flow and the associated combustion, choked nozzle and two-phase flow effects. Solutions are sought as perturbations of reference acoustic modes, solutions of the homogeneous equations (in the absence of mean flow and associated phenomena). That process establishes strong dependence on the acoustic point of view since the final solution can only be small (in the linear sense) perturbation to the acoustic reference mode. The validity of the final solution is thus limited by assumptions which underlie the reference acoustic solution.

The acoustic balance method was first proposed by Hart & McClure [3] and was given its most practical form by Culick [4-6]. The acoustic balance technique belongs to the asymptotic expansion methods. Every variable  $F$  is split into its mean,  $\bar{F}$ , and fluctuating,  $F'$ , parts:

$$F = \bar{F} + F' \quad \text{with } \varepsilon = |F'|/|\bar{F}| \ll 1.$$

$\varepsilon$  is a perturbation parameter that characterizes the instability and is used to split the governing equations into successive powers of  $\varepsilon$ . A second perturbation parameter,  $\bar{M}$ , representing the mean flow Mach number, is used to simplify the equations. Assuming  $\bar{M} \ll 1$  implies that the mean flow remains incompressible, which is a good approximation in the combustion chamber, for practical situations. The use of two perturbation parameters imposes to fix their respective order of magnitude. Considering that the unsteadiness is added to an existing mean flow, it is assumed that:

$$\lim_{\varepsilon, \bar{M} \rightarrow 0} \varepsilon/\bar{M} = 0$$

Then application of this technique to the fluid mechanic equations of mass, momentum and energy balance, leads to the following classes of problems:

$\varepsilon$	$\bar{M}$	Problem
0	$\bar{M}$	Steady, incompressible flow
$\varepsilon$	0	Acoustic, without mean flow
$\varepsilon$	$\bar{M}$	Linear coupling: mean flow-acoustic

The order  $\varepsilon\bar{M}$  is the lower order that permits the description of the instabilities and corresponds to linear equations in  $\varepsilon$ . As a consequence, only the tendencies of infinitesimal perturbations to grow or decay can be determined in the form of a damping coefficient  $\alpha$  ( $F' \propto e^{-\alpha t}$ ). One of the advantages of the linear approach is that it permits to think additively. Indeed, the total damping is the sum of particular  $\alpha_i$ , that can be determined (or corrected) separately:

$$\alpha = \sum_i \alpha_i$$

The acoustic balance approach will be briefly described below, following Culick's paper (see [6]). Assuming that the combustion products form a two-phase mixture (subscript p represents the condensed phase of single class of size  $D_p$ ), let  $\rho_p$  be the apparent particulate density:

$$\rho_p = N m_p ,$$

with  $N$  the number of particles per unit volume and  $m_p$  the mass of a particle. The conservation equations can be written, for an inviscid fluid and inert particles, as follows (the primitive variables are used instead of conservative variables for convenience):

mass:

$$\frac{\partial \rho_g}{\partial t} + \frac{\partial}{\partial x_i} (\rho_g u_i) = 0 \quad (1)$$

$$\frac{\partial \rho_p}{\partial t} + \frac{\partial}{\partial x_i} (\rho_p u_{pi}) = 0 \quad (2)$$

momentum:

$$\rho_g \frac{\partial u_i}{\partial t} + \rho_g u_j \frac{\partial u_i}{\partial x_j} + \frac{\partial p}{\partial x_i} = F_{pi} \quad (3)$$

$$\rho_p \frac{\partial u_{pi}}{\partial t} + \rho_p u_{pi} \frac{\partial u_{pj}}{\partial x_j} = -F_{pi} \quad (4)$$

energy:

$$\rho_g C_V \frac{\partial T}{\partial t} + \rho_g C_V u_i \frac{\partial T}{\partial x_i} + p \frac{\partial u_i}{\partial x_i} = Q_p \quad (5)$$

$$\rho_p C \frac{\partial T_p}{\partial t} + \rho_p C u_{pi} \frac{\partial T_p}{\partial x_i} = -Q_p \quad (6)$$

$F_p$  is the drag force exerted by the particles on a unit volume of gas and  $Q_p$  is the heat transferred to the gas from the particles. For the study of unsteady two-phase flow, it is generally assumed that the two phases are in equilibrium for the steady motions (the unsteady motions will be the cause of unequilibrium). This leads to the following notations:

$u_{pi} = u_i + \delta u_{pi}$  and  $T_p = T + \delta T_p$ , where  $\delta$ 's will have zero mean values. These definitions, together with eqns (4) and (6) lead to the following new inter-phase terms:

$$\delta F_{pi} = -\rho_p \left[ \frac{\partial \delta u_{pi}}{\partial t} + \delta u_{pi} \frac{\partial u_j}{\partial x_j} + u_i \frac{\partial \delta u_{pj}}{\partial x_j} \right] \quad (7)$$

$$\delta Q_p = -\rho_p C \left[ \frac{\partial \delta T_p}{\partial t} + \delta u_{pi} \frac{\partial T}{\partial x_i} + u_i \frac{\partial \delta T_p}{\partial x_i} \right] \quad (8)$$

Finally, defining the mixture properties as:

$$\kappa = \rho_p / \rho_g$$

$$\rho^* = (1 + \kappa) \rho_g$$

$$C_V^* = (C_V + \kappa C) / (1 + \kappa)$$

$$R^* = R_g / (1 + \kappa): \text{mixture perfect gas constant}$$

$$p^* = p = R^* T / \rho^* = RT / \rho: \text{static pressure}$$

$$\gamma^* = 1 + R^* / C_V^* = \gamma(1 + \kappa C / C_p) / (1 + \kappa C / C_V)$$

$$a^* = \left[ \frac{1 + \kappa C / C_p}{(1 + \kappa)(1 + \kappa C / C_V)} \right]^{1/2} a_g$$

equations (3) and (5) can be rewritten for the mixture:

$$\rho^* \frac{\partial u_i}{\partial t} + \rho^* u_j \frac{\partial u_i}{\partial x_j} + \frac{\partial p}{\partial x_i} = \delta F_{pi} \quad (9)$$

$$\rho^* C_V^* \frac{\partial T}{\partial t} + \rho^* C_V^* u_i \frac{\partial T}{\partial x_i} + p \frac{\partial u_i}{\partial x_i} = \delta Q_p \quad (10)$$

Then eqn (10) can be written for the pressure:

$$\frac{\partial p}{\partial t} + u_i \frac{\partial p}{\partial x_i} + \left( \frac{R^*}{C_V^*} + 1 \right) p \frac{\partial u_i}{\partial x_i} = \frac{R^*}{C_V^*} \delta Q_p \quad (11)$$

At this point it is interesting to note, that under the assumptions of a steady state motion and of inert particles, eqn. (2) gives:

$$\frac{\partial}{\partial x_i} (\kappa \rho_g u_i) = 0$$

which, using eqn. (1), leads to:

$$u_i \frac{\partial}{\partial x_i} (\kappa) = 0$$

implying that  $\kappa$  is conserved on any streamline. Since  $\kappa$  is uniform on the propellant surface,  $\kappa$  is uniform throughout the chamber.

The next step is to develop eqns. (9) and (11) to first order in  $\varepsilon$  and  $\bar{M}$ . It must be noted that the inter-phase equilibrium hypothesis permits to assimilate the mixture (superscript \*) and the steady gas motion (notation  $\bar{\phantom{x}}$ ).



Steady state:

$$\frac{\partial}{\partial x_i} (\overline{u_i}) = 0 + O(\overline{M}^2)$$

$$\frac{\partial}{\partial x_i} (\overline{p}) = 0 + O(\overline{M}^2)$$

First order:

$$\frac{\partial p'}{\partial t} + \overline{u_i} \frac{\partial p'}{\partial x_i} + \gamma \overline{p} \frac{\partial u_i'}{\partial x_i} = \frac{R}{C_V} \delta Q_p' \quad (12)$$

$$\overline{p} \frac{\partial u_i'}{\partial t} + \frac{\partial p'}{\partial x_i} = \delta F_{pi}' - \overline{p} \left( \overline{u_j} \frac{\partial u_i'}{\partial x_j} + u_j' \frac{\partial \overline{u_i}}{\partial x_j} \right) \quad (13)$$

Then, taking the time derivative of eqn. (12) and combining with the divergence of eqn. (13) and assuming harmonic motions ( $F' = \tilde{F} \exp(i\omega t)$ ), one gets an inhomogeneous Helmholtz's equation for  $p$ . This equation is valid in the interior domain  $\Omega$  where the mean flow can be assumed incompressible. Its boundary conditions are obtained by taking the scalar product of eqn. (13) with the outward unit normal vector,  $n_i$ , along the chamber boundaries:

$$\frac{\partial^2 \tilde{p}}{\partial x_i \partial x_i} + k^2 \tilde{p} = \tilde{h} \quad (14)$$

$$n_i \cdot \frac{\partial \tilde{p}}{\partial x_i} = -\tilde{f} \quad (15)$$

with:

$$k = (\omega + i\alpha)/a$$

$$\begin{aligned} \tilde{h} = & i \frac{\omega}{a} \frac{\overline{u_i}}{a} \frac{\partial \tilde{p}}{\partial x_i} - i(\gamma - 1) \frac{\omega}{a^2} \delta \tilde{Q}_p + \frac{\partial}{\partial x_i} (\delta \tilde{F}_{pi}) \\ & - \overline{p} \frac{\partial}{\partial x_i} \left( \overline{u_j} \frac{\partial \tilde{u_i}}{\partial x_j} + \tilde{u_j} \frac{\partial \overline{u_i}}{\partial x_j} \right) \end{aligned} \quad (16)$$

$$\tilde{f} = i\omega \overline{p} n_i \tilde{u_i} - n_i \delta \tilde{F}_{pi} - \overline{p} n_i \left( \overline{u_j} \frac{\partial \tilde{u_i}}{\partial x_j} + \tilde{u_j} \frac{\partial \overline{u_i}}{\partial x_j} \right) \quad (17)$$

For the unperturbed case (rigid boundaries <sup>(\*)</sup>, no mean flow and no particles), one has classically:

$$\frac{\partial^2 \tilde{p}_N}{\partial x_i \partial x_i} + k_N^2 \tilde{p}_N = 0 \quad (18)$$

(\*) This assumption is justified in most cases, except the cases with “long nozzles” where the nozzle admittance must be taken into account in eq. (19) (see ref. [7]).

$$\mathbf{n}_i \cdot \frac{\partial \tilde{\mathbf{p}}_N}{\partial \mathbf{x}_i} = 0 \quad (19)$$

Combining eqns. (14) to (19) and taking a volume average over the domain  $\Omega$ , one can arrive, after some tedious algebra, for an expression (eqn. 20) for the perturbed wave number,  $k$ , valid at first order, and making use of the unperturbed eigen mode of the chamber:

$$\begin{aligned} (k^2 - k_N^2) E_N^2 &= -ik_N \int_{\partial\Omega} (A_n + \overline{M}_n) \tilde{\mathbf{p}}_N^2 dS \\ &- \int_{\Omega} \delta \tilde{F}_{pi} \frac{\partial \tilde{\mathbf{p}}_N}{\partial \mathbf{x}_i} dV - i(\gamma - 1) \frac{k_N}{a} \int_{\Omega} \delta \tilde{Q}_p \tilde{\mathbf{p}}_N dV \end{aligned} \quad (20)$$

The following definitions are used:

$$E_N^2 = \int_{\Omega} \tilde{\mathbf{p}}_N^2 dV$$

$$A_n = \bar{\rho} a \frac{\tilde{u}_i n'_i}{\tilde{p}}$$

$$M_n = \frac{\bar{u}_i n'_i}{a}$$

where  $\mathbf{n}'_i$  is the inward pointing unit normal vector.

It must be noted that to arrive at equation (20) one has to assume that the vector  $\tilde{\mathbf{u}}_i$  is proportional to the gradient  $\partial \tilde{\mathbf{p}}_N / \partial \mathbf{x}_i$ , imposing an irrotational field for the unsteady velocity. This assumption bears several limitations for the use of the acoustic balance. Indeed recent works have demonstrated that the unsteady velocity field may be highly rotational, as a consequence of the propellant side injection [e.g. 8-11]. Recent works propose a modification of the acoustic balance technique [10] to account for unsteady vorticity. It is outside the scope of this paper to discuss that matter. It must also be said that in situations where vortex shedding takes place, the assumption of an irrotational velocity field is also incorrect.

Equation (20) can be split in its real and imaginary parts to give the following equations for the frequency shift and the damping coefficient, brought by the perturbation (assuming that  $\alpha^2 \ll \omega^2$ ):

$$\begin{aligned} \omega - \omega_N &= \frac{a}{2E_N^2} \int_{\partial\Omega} \text{Im}(A_n) \tilde{\mathbf{p}}_N^2 dS \\ &- \frac{a}{2k_N E_N^2} \int_{\Omega} \text{Re} \left( \delta \tilde{F}_{pi} \frac{\partial \tilde{\mathbf{p}}_N}{\partial \mathbf{x}_i} \right) dV \\ &- (\gamma - 1) \frac{1}{2E_N^2} \int_{\Omega} \text{Im}(\delta \tilde{Q}_p \tilde{\mathbf{p}}_N) dV \end{aligned} \quad (21)$$

$$\begin{aligned} \alpha &= \frac{-a}{2E_N^2} \int_{\partial\Omega} (\text{Re}(A_n) + \overline{M}_n) \tilde{\mathbf{p}}_N^2 dS \\ &- \frac{a}{2k_N E_N^2} \int_{\Omega} \text{Im} \left( \delta \tilde{F}_{pi} \frac{\partial \tilde{\mathbf{p}}_N}{\partial \mathbf{x}_i} \right) dV \\ &- (\gamma - 1) \frac{1}{2E_N^2} \int_{\Omega} \text{Re}(\delta \tilde{Q}_p \tilde{\mathbf{p}}_N) dV \end{aligned} \quad (22)$$

### Particular Contributions to the Acoustic Balance

The last two volume integrals of the above equations concern the particulate damping and will be discussed in a following section. Concentrating on eqn. (22), and discarding the particulate dampings, usual form will be given. The first surface integral can be broken over the following surfaces:

- Propellant surfaces: due to the propellant combustion,  $M_n$  represents the injection Mach number,  $M_{inj}$ , and  $A_n$  the propellant admittance. It is common practice to use the propellant burning rate response,  $R_{MP}$ , instead of the admittance. These two quantities are linked by the following relationship:

$$R_{MP} = \frac{v'_c / \bar{v}_c}{p' / \bar{p}} = \frac{\rho' / \bar{\rho}}{p' / \bar{p}} + \frac{\bar{p}}{a M_{inj}} \frac{u'_i \cdot n'_i}{p'}$$

$$\Rightarrow R_{MP} = \frac{1}{\gamma M_{inj}} [M_{inj} + A_n]$$

A global response is sometimes defined as:  $R_c = R_{MP} + R_{TP}$ , with  $R_{TP}$  being the temperature response. Assuming isentropic oscillations leads to:

$$R_c = R_{MP} + \frac{T' / \bar{T}}{p' / \bar{p}} = R_{MP} + \frac{\gamma - 1}{\gamma}$$

Then, assuming that the propellant combustion does not depend one the location, the combustion term  $\alpha_c$  can be obtained as:

$$\alpha_c = -\gamma a M_{inj} \text{Re}(R_{MP}) \frac{\int_{S_{inj}} \tilde{p}_N^2 dS}{2 \int_{\Omega} \tilde{p}_N^2 dV} \quad (23)$$

- Inert walls: their contributions are obviously zero.
- Nozzle entrance plane: due to different normal vectors orientations,  $M_n$  represents  $-M_L$ , and  $A_n$  represent  $-A_L$ , with  $M_L$  and  $A_L$  being the nozzle inlet Mach number and acoustic admittance respectively. Assuming uniform properties across the nozzle entrance plane, the nozzle term is broken into the following convective,  $\alpha_{NC}$ , and radiative,  $\alpha_{NR}$ , parts:

$$\alpha_{NC} = a \bar{M}_L \frac{\int_{S_L} \tilde{p}_N^2 dS}{2 \int_{\Omega} \tilde{p}_N^2 dV} \quad (24)$$

$$\alpha_{NR} = a \text{Re}(A_L) \frac{\int_{S_L} \tilde{p}_N^2 dS}{2 \int_{\Omega} \tilde{p}_N^2 dV} \quad (25)$$

Once the propellant and nozzle properties are known, evaluating the motor linear stability is only a question of computing the reference acoustic mode, solution of eqns. (18) and (19), and evaluating the different stability integrals appearing in  $\alpha_c$ ,  $\alpha_{NC}$ , and  $\alpha_{NR}$ . The resulting damping coefficient will then be  $\alpha = \alpha_c + \alpha_{NC} + \alpha_{NR}$ .

This will be illustrated for a simple cylindrical port motor displayed in fig. 3, and for the case of the  $q^{\text{th}}$  longitudinal mode.

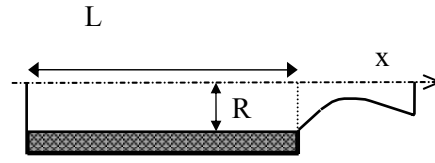


**Figure 3: Simple Cylindrical Motor.**

The following equations are used:

$$S_{inj} = 2\pi RL, S_L = \pi R^2, \Omega = \pi R^2 L$$

$$M_L = \frac{S_{inj}}{S_L} M_{inj}, M_{inj} = \frac{V_{inj}}{a}$$

$$\tilde{p}_N = \tilde{p}_{N0} \cos(k_N x) \text{ with } k_N = q \frac{\pi}{L}$$

Finally:

$$\alpha_c = -\gamma \frac{V_{inj}}{R} \text{Re}(R_{MP})$$

$$\alpha_{NC} = \frac{a M_L}{L} = \frac{2 V_{inj}}{R}$$

$$\alpha_{NR} = \frac{a \text{Re}(A_L)}{L}$$

To estimate the effectiveness of the dampings,  $\alpha$  must be compared to the frequency,  $f_q = q a / (2L)$ , so that:

$$\frac{\alpha_c}{f_q} = -\gamma \frac{2}{q} \frac{L}{R} M_{inj} \text{Re}(R_{MP})$$

$$\frac{\alpha_{NC}}{f_q} = \frac{2}{q} M_L = \frac{2}{q} \frac{2L}{R} M_{inj}$$

$$\frac{\alpha_{NR}}{f_q} = \frac{2}{q} \text{Re}(A_L)$$

It must be noted that for short nozzles, it is common to approximate the real part of the nozzle admittance,  $A_L$ , by its value derived from a quasi-steady analysis:

$$\frac{P A_c}{C^*} = (\rho U A)_L \Rightarrow \frac{p'}{\bar{P}} - \frac{1}{2} \frac{T'}{\bar{T}} = \frac{\rho'}{\bar{\rho}} + \frac{u'}{\bar{U}}$$

$$\text{with: } \frac{T'}{\bar{T}} = \frac{p'}{\bar{P}} - \frac{\rho'}{\bar{\rho}}, \quad \frac{\rho'}{\bar{\rho}} = \frac{1}{\gamma} \frac{p'}{\bar{P}} \quad \text{and} \quad \bar{P} = \frac{\bar{\rho} a^2}{\gamma}$$

$$\text{hence: } A_L = \bar{\rho} a \frac{u'}{p'} = \frac{\gamma-1}{2} \bar{M}_L$$

$$\Rightarrow \text{Re}(A_L) = \frac{\gamma-1}{2} \bar{M}_L$$

This permits to evaluate the relative order of magnitude of equations (24) et (25). Assuming  $\gamma \approx 1.2$ , it is found that the radiative term represents roughly 10% of the convective one. The fact that  $\text{Re}(A_L)$  is a small number validates the assumption that the nozzle entrance plane behaves much like a rigid wall.

Then evaluating the resulting  $\alpha$ , one gets in this simple case:

$$\frac{\alpha}{f_q} = \frac{2}{q} \frac{L}{R} M_{inj} \left[ -\gamma \text{Re}(R_{MP}) + 2 + \frac{\gamma-1}{2} \right] \quad (26)$$

From this equation it appears that unless  $\text{Re}(R_{MP})$  is larger than  $(\gamma+3)/2\gamma (\approx 1.75)$  stability will be predicted. This limit will be even higher when the flow-turning correction will be added to the acoustic balance (see next section).

In more complex situations, the stability integrals must be carried out numerically, as well as the determination of the reference acoustic mode. It can be seen from eqns. (23) and (24-25) that the location where the combustion takes place and/or where the nozzle is located with respect to the reference acoustic mode will affect the global balance. In particular, the most famous T burner, with its propellant samples at the chamber ends and its nozzle at the mid-chamber position, will favor motor instability (which is what it was designed for).

### Flow Turning Issue

The flow turning issue is a long debated subject (e.g. see [1, 2, 6, 8, 10, 12, 13]). It appeared from the fact that the results of the 1D acoustic balance are different from the 3D ones. An additional term is found in the form of a surface integral over the burning surface:

$$\alpha_{FT} = \frac{a}{2k_N^2 E_N^2} \int_{S_{inj}} \overline{M}_{inj} \left( \frac{d\tilde{p}_N}{dx} \right)^2 dS \quad (27)$$

This term was extended to the 3D analysis by Culick [6]. It derives from the condition of a no-slip boundary condition that can be freely imposed in 1D whereas the 3D approach forces an irrotational unsteady field. This was interpreted as a viscous effects, due to acoustic boundary layers. However, a simplified viscous treatment, near the injecting surface, led to a different expression [8], resulting from the “apparent” propellant admittance. Indeed, the actual propellant admittance has to be corrected from the displacement effect of the viscous layers. In the case of the relatively strong blowings encountered in SRM, this correction had a limiting value, independent of the viscosity, which was troubling. This term, supposed to replace the  $\alpha_{FT}$  term, was:

$$\alpha_{BL} = \frac{a}{2E_N^2} \int_{S_{inj}} \overline{M}_{inj} (\tilde{p}_N)^2 dS \quad (28)$$

Please note that in the case of a pure cylindrical motor, both eqns. (27) and (28) give the same result, adding to the trouble. The discussion was further fed by full numerical solutions of the unsteady Navier-Stokes equations [9, 11] that clearly showed that the unsteady velocity field was clearly rotational, invalidating both the 1D and the 3D approaches and the  $\alpha_{FT}$  term, but also that the so-called acoustic boundary layers were very thick, invalidating the admittance correction approach and the  $\alpha_{BL}$  term. In several recent papers [e.g. 14], Majdalani *et al.* revisited the problem of unsteady vorticity in acoustic solutions and proposed a unified mathematical framework.

In any cases, most researchers agree to the fact that the uncorrected acoustic balance, as expressed in eqn. (26), underestimates the motor stability. Indeed, for the simple cylindrical motor, one gets:

$$\frac{\alpha_{FT}}{f_q} = \frac{\alpha_{BL}}{f_q} = \frac{2}{q} \frac{L}{R} M_{inj}$$

leading to the following expression:

$$\frac{\alpha}{f_q} = \frac{2}{q} \frac{L}{R} M_{inj} \left[ -\gamma \text{Re}(R_{MP}) + 3 + \frac{\gamma-1}{2} \right] \quad (29)$$

which sets the stability limit to  $\text{Re}(R_{MP})$  larger than  $(\gamma+5)/2\gamma (\approx 2.58)$ , which is a rather large value for the real part of the response function. One may then conclude, that if the combustion is the only driving mechanism, most motors should be stable on their longitudinal modes, which is unfortunately not the case. For transverse modes and especially the tangential modes, the above analysis leads to less marked conclusions, in particular due to the nozzle terms which contributes to only limited losses.

## Two-Phase Flows

Since most motors use metallized propellants, the combustion products carry some amount of condensed phase products, such as alumina droplets. These will add to the motor stability. In fact, one of the reasons to load propellants with metal powder, such as aluminum, is to increase the stability of the motors (another reason being the benefit of increased specific impulse).

Evaluation of the particulate terms in eqns. (21) and (22), can be done providing that ad-hoc laws are supplied for the drag force and the heat transferred between phases. Reference [15] describes the problem and proposes solution methods. It is common practice to evaluate the two-phase flow terms for the simplified Stokes regimes, valid for small (less than unity) particular Reynolds numbers ( $\text{Re}_p = \rho D_p \Delta U_p / \mu$ , where  $\Delta U_p$  is the velocity difference between the two phases). For low amplitude oscillations, this is consistent with the equilibrium hypothesis, since then:

$$(\text{Re})_p = \frac{\rho_g D_p |\delta \tilde{\mathbf{u}}_p|}{\mu}$$

Under these conditions, the drag coefficient takes the well known value of:

$$C_D = 24 / (\text{Re})_p$$

and the convective heat transfer coefficient is taken as:

$$h' = 2\lambda / D_p \text{ (Nusselt number } = 2),$$

This leads to the following linear relations:

$$\delta \mathbf{F}_p = N_p (3\pi \mu D_p) \delta \mathbf{u}_p$$

$$\delta Q_p = N_p (2\pi \lambda D_p) \delta T_p$$

## Motor Flow Instabilities – Part 1

At first order, eqns. (7) et (8) lead to:

$$|\delta \mathbf{u}_p| = |\delta \mathbf{u}_p|_0 e^{-\frac{t}{\tau_v}} \quad \text{with} \quad \tau_v = \frac{\rho_{ps} D_p^2}{18\mu}$$

$$|\delta T_p| = |\delta T_p|_0 e^{-\frac{t}{\tau_T}} \quad \text{with} \quad \tau_T = \frac{3}{2} \text{Pr} \frac{C}{C_p} \tau_v$$

Finally, expressing  $\delta F_p$  et  $\delta Q_p$  as functions of the fluctuating velocity and temperature (which, at first order, can be directly linked to  $\partial p_N / \partial x$  and  $p_N$ , one gets:

$$\delta F_{pi} = \kappa \frac{1 - i\omega\tau_v}{1 + (\omega\tau_v)^2} \frac{\partial \tilde{p}_N}{\partial x_i}$$

$$\delta Q_p = -\kappa \omega \frac{C}{C_p} \frac{i + \omega\tau_T}{1 + (\omega\tau_T)^2} \tilde{p}_N$$

These are then incorporated into eqns. (21) et (22). With some further approximations, valid for small  $\kappa$  and for  $C/C_p$  et  $C/C_v$  close to unity, the particular damping term can be expressed as:

$$\alpha_p = \kappa \frac{\omega}{2} \left[ \frac{\omega\tau_v}{1 + (\omega\tau_v)^2} \frac{\int_{\Omega} \left( \frac{d\tilde{p}_N}{dx} \right)^2 dV}{k_N^2 \int_{\Omega} \tilde{p}_N^2 dV} + (\gamma - 1) \frac{C}{C_p} \frac{\omega\tau_T}{1 + (\omega\tau_T)^2} \right] \quad (30)$$

Please note that on the contrary to the preceding terms, this expression involves a volume effect.

For the simple cylindrical motor, this expression becomes:

$$\alpha_p = \kappa \frac{\omega}{2} \left[ \frac{\omega\tau_v}{1 + (\omega\tau_v)^2} + (\gamma - 1) \frac{C}{C_p} \frac{\omega\tau_T}{1 + (\omega\tau_T)^2} \right]$$

and finally:

$$\frac{\alpha_p}{f_q} = \kappa \pi \left[ \frac{\omega\tau_v}{1 + (\omega\tau_v)^2} + (\gamma - 1) \frac{C}{C_p} \frac{\omega\tau_T}{1 + (\omega\tau_T)^2} \right]$$

Neglecting the thermal term, the optimum damping is obtained for  $\omega\tau_v = 1$ , which leads to:

$$(\alpha_p)_{\text{opt}} = \kappa \frac{9\mu}{2\rho_{ps} D_p^2} \quad \text{and} \quad (f)_{\text{opt}} = \frac{9\mu}{\pi\rho_{ps} D_p^2}$$

$$(D_p)_{\text{opt}} = \sqrt{\frac{9\mu}{\pi\rho_{ps} f}}$$

This relation can be used to adjust the propellant loading to damp potentially unstable modes (most of the time, the feared tangential modes) by selecting the proper particle sizes.

## Conclusion/Limitations

The above sections described the engineer tools for predicting motor stability. In practical situations, which depart from the simple cylindrical motor considered here, this task involves the determination of the reference acoustic modes and the evaluation of the stability integrals. Inputs to the model are the propellant response function, the nozzle admittance and the particular phase sizes. These can be obtained from experiments, dedicated to that characterization effort, and bear some uncertainties, sometimes quite large, due to the complex physical mechanisms involved. This, added to the fact that some difficulties arise from the formulation itself (e.g. how to express the flow-turning loss or the nozzle admittance in complex geometries), makes the acoustic balance a **“useful tool of limited validity”**. It is not surprising that stability is predicted most of the time, while unstable motors keep haunting the rocket engineers’ nights.

## FLOW STABILITY

### Presentation

From what precedes, it is clear that some sources of instability are missing from the acoustic balance approach. Flandro and Jacobs [16] were the first to mention the “vortex-shedding” as a possible additional driving to the motor stability balance. It was viewed as a coupling between a shear layer instability (in the hydrodynamic sense) and the chamber acoustic. First works considered simple correlations in term of critical Strouhal numbers (see [17] for a detailed presentation). These Strouhal numbers were based on the mean axial velocity ( $U$ ) and either on the port diameter ( $D$ ):  $(St)_D$ , or on the stand-off distance between the vortex generation point and its impact,  $\ell$ ,  $(St)_\ell$ :

$$(St)_D = fD/U \text{ and } (St)_\ell = f\ell/U$$

References [18-24] present interesting attempts to use correlations of this type. However, it must be stressed that such correlations have a limited predictive merit and can be compared to the celebrated “age of the captain” formula (mast height divided by the ship speed): all the difficulty lies in the proportionality constant which has no universal quality. Reference [20] goes one step further in using the Rossiter’s formula to correlate the observed frequencies. This approach uses the relative time delays of the vortex emission to the acoustic feedback. The figure hereafter illustrates this point of view.

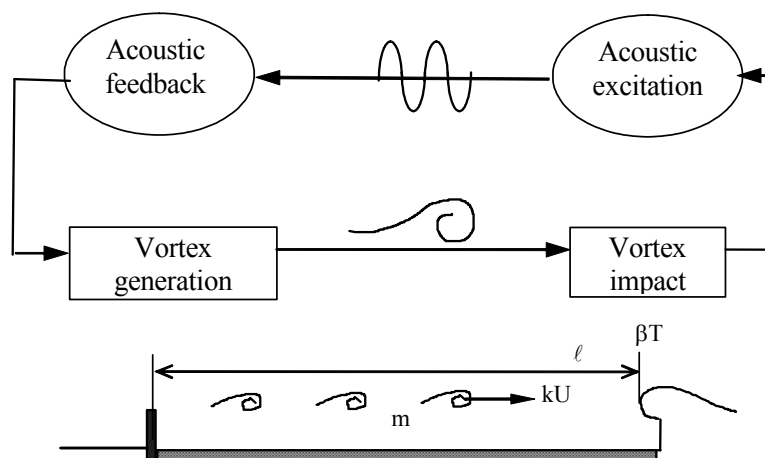


**Figure 4: Illustration of the Vortex-Shedding Phenomenon.**



## Motor Flow Instabilities – Part 1

Let  $T$  be the time period of the vortex-shedding,  $k$  the ratio of vortex displacement velocity to the mean axial flow velocity,  $U$ ,  $\beta$  an empirical constant representing the time delay between vortex impact and acoustic wave emission and  $m$  the number of vortices on distance  $\ell$ , then one gets:

$$mT = \ell/kU + \ell/c + \beta T$$

$k$  and  $\beta$  are empirical constants that must be case adjusted from the measurement of the frequency.

Reference [20] uses this relationship to express  $(St)_\ell$  as:

$$(St)_\ell = \frac{m-\beta}{M+1/k}$$

leading to:  $f = \frac{U}{\ell} \frac{m-\beta}{M+1/k} \approx k \frac{U}{\ell} (m - \beta)$  (31)

$M$  is the Mach number associated to  $U$  and can be neglected before  $1/k$  (always greater than 1).

Application of this formula to the Titan SRMU leads to values of  $m$  in the range 5-12, and to  $k = 0.58$  and  $\beta = 0.25$ , which is in reasonable agreement with previous works (see [20]).

It is important to stress that such an approach is simplified and cannot be fully predictive. However it turns out to be quite useful in interpreting firing test measurements.

The most complete approach to this problem is that of Flandro [22]. Vortex properties (wave length, displacement speed) are derived from the hydrodynamic stability analysis of the velocity profile at the origin of vortex-shedding. The impact mechanisms are modeled through a localized volumetric force. References [17, 23-25] present applications of this method to the Ariane 5 MPS P230 solid boosters. The aim is to derive a vortex-shedding additional term,  $\alpha_{VS}$ , to the acoustic balance results. However, non realist values are obtained (due to the strong linear growth of the vortices) and the method was limited to a qualitative analysis (driving or damping effects) that is based on the phase difference between the vortices at impact and the acoustic field. This method will not be further detailed here, although it represents a unique attempt to quantify the Rossiter's equation from first principles, because it was found to be extremely sensitive to unknown details, such as the precise location of the vortex origin. The interested readers are referred to references [22-25 and 17].

Looking back at the acoustic balance approach, it is interesting to look at the implications of rotational fields on the final equations (see [26, 17]). Indeed, assuming that the unsteady velocity is no longer aligned with the gradient of the acoustic pressure, additional terms result from the linearization of the  $\mathbf{u} \cdot \nabla \mathbf{u}$  term in the RHS of eqn. (20). These terms take the following form:

$$\bar{\rho} \left\{ \int_{\Omega} k_N^2 [\bar{\mathbf{u}} \cdot (\tilde{\mathbf{u}} - \tilde{\mathbf{u}}_N)] \tilde{p}_N dV + \int_{\Omega} (\bar{\boldsymbol{\omega}} \wedge \tilde{\mathbf{u}}) \cdot \nabla \tilde{p}_N dV + \int_{\Omega} (\tilde{\boldsymbol{\omega}} \wedge \bar{\mathbf{u}}) \cdot \nabla \tilde{p}_N dV \right\}$$

These integrals are difficult to evaluate in general and need to know the flow organization in the volume of the motor. However, it is interesting to note that the last integral implies unsteady vorticity and can be related to the vortex-shedding phenomenon. For a two-dimensional flow its integrand reduces to:

$$-\tilde{\omega}_z \bar{v} \frac{\partial \tilde{p}_N}{\partial x}$$

It can be argued that this integrand takes significant values at localized points inside the motor chamber, such as the nozzle entrance where  $\tilde{\omega}_z$  and  $\bar{v}$  are large, thus providing a natural way to introduce the

coupling between the vortical and the acoustic fields. The volume integral can then be reduced to a surface integral at the vortex “impact” point as proposed by Flandro.

### **Intrinsic Non-Linear Nature**

Attempts to complement the basic acoustic balance approach are impeded by difficulties linked to the departure of the unsteady field, in particular the velocity field, from the pure acoustic vision. Indeed, the flow-turning debate illustrates the difficulty in incorporating unsteady vorticity in the acoustic framework, while the vortex-shedding issue exemplifies the difficulties in taking care of flow instabilities in the linear framework.

The fact that the mean flow can become unstable by its own is now an accepted result. The fact that this unstable behavior cannot easily fit into the acoustic framework is also becoming evident. One of the reasons that one can invoke is that flow instability evolves on its own, as an independent mechanism, with no need to an acoustic reference. The attempts to treat separately these two independent mechanisms from variable decomposition: mean and fluctuating flows, with the fluctuating flow composed of an compressible irrotational (acoustic component) and an incompressible rotational (vortical component) components, at the basis of Flandro’s approach, failed to provide useful results. The reason of failure lied not in the necessary coupling equations, which could be written, but rather in the difficulty to describe the vortical evolutions. Indeed, vortical flow can be characterized in its linear regime (initial growth of instability waves) with proven methods (Orr-Sommerfeld type approaches) but growth rates in this early linear regime are quite high and the vortical field rapidly enters some form of non-linear regimes which are much more complex to model. The fact that in most situations the interactions between the two unsteady fields occur when the vortical fields has become non-linear, may explain the failure of the above mentioned approaches.

Most of the time, **observable vortices are the results of a non-linear growth process**. As a consequence, our knowledge of such vortices and of their dependencies on the known parameters is blurred by the non-linear growth stage of initial unstable vortical waves, a process which most of the time remains beyond our present understanding. However it is of **major importance to better understand the initial destabilisation mechanisms**, simply because they have definite frequency signatures and sensitivities to flow characteristics which must be known in order to understand their potential effectiveness to couple with acoustic waves and produce harmful vortices. Controlling the early stage of flow instabilities is undoubtedly an effective mean of avoiding unwanted motor instabilities driven by some form of vortex-shedding. **In that view the knowledge of flow stability characteristics is an essential prerequisite to any attempt in controlling motor flow driven instabilities**. This is detailed in the second paper devoted to the stability theory.

### **Model Requirements**

From what precedes, it is clear that if motor flow driven instabilities have to be predicted, one has to rely on a model that has the ability to describe, in the same framework, both the acoustic waves and the vortical waves (including non-linear interactions). From that point of view, the full numerical solution of the compressible Navier-Stokes equations provides the needed framework.

However, since the instabilities can be viewed as resonance mechanisms that involve the motor chamber acoustic modes and unstable couplings of physical phenomena linked to the mean flow, the Navier-Stokes equations have to be completed to include all the needed phenomena. Considering the nature of the solid propellant rocket internal flows, identified physical mechanisms are:

- the mean flow itself, including sheared flows, nozzle flows, and turbulence,
- the propellant combustion at the burning surface,

## Motor Flow Instabilities – Part 1

---

- the combustion of aluminum droplets carried by the flow,
- the structure motions (as possibly affecting the mean and unsteady flows).

Finally, the model should be able:

- a) to propagate the acoustic waves,
- b) to describe the details of the internal flow, including the capture of acoustically forced vorticity waves as well as flow instabilities and their non-linear growth,
- c) to include some form of condensed phase model (inert and reactive),
- d) to couple with propellant combustion models,
- e) to couple with solid mechanic models.

This analysis concluded that full solutions of the compressible unsteady Navier-Stokes equations, including reactive two-phase flow treatments should be sought. Indeed, as already mentioned, such solutions have the capability to describe both the acoustic and flow vorticity, without the need to separate the solution in several flow components. We have underlined that this poses some problems for describing each component in a compatible way. Further, such a model could be coupled through its boundary conditions to propellant combustion models and solid mechanic codes, to permit a complete description of the identified mechanisms. This would then provide an unprecedented tool for analyzing motor instabilities.

However, such a solution would necessarily rely on a numerical solution of the equations and some concerns were raised about the ability of the numerical procedure to faithfully describe the solution, due to numerical errors and grid size requirements. As a consequence, it was agreed that such a solution method should pass through a severe validation procedure before it could be safely used in predicting motor stability.

This validation requirement posed in turn some constraints which were the need for detailed measurements in known situations to provide the data against which the numerical results would be validated. This was quite a new constraint and it promoted a series of unique research works, sometimes of ingrate nature, that had to be performed to sustain the construction of this new tool. Here “ingrate” must be understood, not as scientifically uninteresting works but rather as far from actual motor applications and thus implying difficulties in being funded and fully appreciated by program managers. However, such works were essential and ranked from:

- Cold flow simulators in which detailed velocity measurements could be performed and compared to numerical simulation results,
- Analytical solutions of unstable flow regimes,
- Dedicated lab scale motors with high quality and numerous measurements to gain real firing tests data,
- Meticulous characterization efforts to provide the model inputs. These comprised condensed phase characterizations, details of the propellant composition, including characterizations of AP and aluminum size distributions, and unsteady propellant combustion responses function determinations,
- Dedicated models for combustion mechanisms and fluid-structure couplings,
- Dedicated and documented test cases for model evaluations.

Such works have been carried out in Europe thanks to the Ariane 5 related programs and represent a valuable asset for the development of a comprehensive model for motor stability predictions. For the first time,

at the end of that research effort, actual unstable motor behaviors could be simulated numerically and produced results that agreed both in frequency and in oscillatory amplitude, with motor measurements. Results of such quality were judged unattainable at the start of the research effort and are worth to be celebrated. Of course much remains to be done yet, to guarantee the capability of a priori predictions from scratch (i.e. before any firings are performed).

## **STABILITY THEORY**

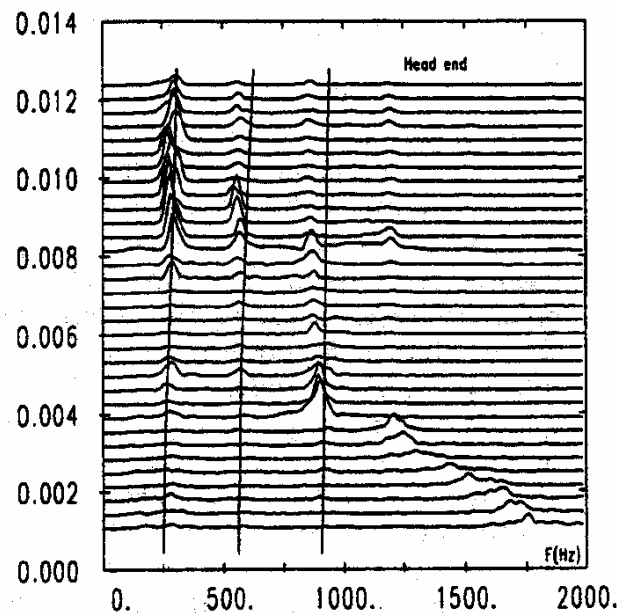
This part is described in details in the second paper.

## **DEALING WITH FLOW STABILITY**

### **Experimental Evidences**

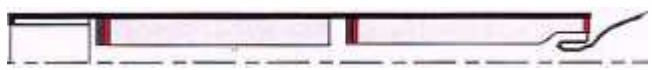
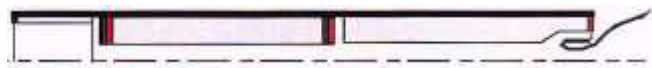
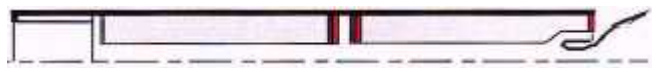
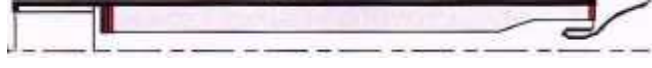

From early works of Flandro *et al.*, it was expected that flow instabilities could drive unstable motors. In particular, it was stressed that inflectional velocity profiles, as created above protruding obstacles or at propellant grain discontinuities could be at the origin of unstable flows, prone to produce vortex-shedding driven instabilities. The works carried out in the USA, relative to the Space Shuttle and the Titan boosters, clearly demonstrated that vortex-shedding could drive the first longitudinal modes of the motor [27-30, 18-22]. The works of Dunlap *et al.* [19] established that for such large segmented space boosters, protruding inhibitor rings, such those created by the front ends thermal insulations of propellant segments (typically the aft segments), could be at the origin of highly sheared flow that produced periodic vortex-shedding driving the motors unstable. This was also observed in Ariane 5 boosters [31]. The resulting mild pressure oscillations were disturbing since all these motors were predicted stable by the acoustic balance method and more annoying, they produced significant thrust oscillations, due to high pressure to thrust ratio (of the order of 10). This high value of the ratio can be straightforwardly explained from geometric and phase relationships. Moreover, the low frequencies associated with these large motors (recall that  $f_{1L} \approx a/2L$ ) rendered such oscillations undesirable since they were able to couple to the structural modes and thus to propagate easily to the launcher structure and payloads.

The vortical origin of these oscillations can be traced to their particular frequency signatures. Indeed it was observed that instabilities followed peculiar frequency tracks, showing decreasing frequencies and sudden jumps around the pure acoustic frequency. For example, the figure below shows the time evolution of the head end pressure power spectral density for one subscale firing. The particular frequency tracks around chamber acoustic mode frequencies (solid lines) is evident. The decrease of the frequency during motor burn was viewed as an indication of the driving being the result of flow instabilities, linked to the mean flow axial velocity. Indeed in most solid propellant motors the axial velocity continuously decreases, due to increasing motor port area, as propellant burns out. The jumps were viewed as system adaptation to changing conditions: when the vortex driving frequency falls too far away from the acoustic frequency, an increase in the number of vortices occurs (see eqn. 31) to bring back the driving frequency in the acoustic range. Such behaviors could not be explained by the acoustic balance approaches and were considered as evidence of an hydrodynamic origin of the oscillations.



**Figure 5: Typical Frequency Tracks for Flow Driven Instabilities (LP3 E Firing).**

In Europe the development of the Ariane 5 segmented solid rocket motor promoted researches in that area, looking to unstable behaviors of segmented motors. A subscale motor was designed from a simplified, 1/15<sup>th</sup> scale, geometry of Ariane 5 P230 MPS solid rocket motor. Cylindrical propellant grains were used and a non-aluminized propellant was chosen. Since the emphasis was put on flow driven instabilities it was thought that details of the combustion should be of secondary importance. The overall P230 segmentation scheme was reproduced with a propellant loading composed of three segments: a short head end segment of limited burn time (roughly 20% of total burn time), two longer mid and aft segments. As in the full scale motor, a submerged nozzle assembly was retained. This motor was named LP3 and five configurations were fire tested [24, 32]. For each configuration, two firings were performed to check for reproducibility. The configurations differed between each other by segment arrangements, as depicted in figure 6 below.

LP3 A		Nominal configuration: mid and aft segments inhibited on their forward ends
LP3 B		Inhibitor rings on both ends of the mid-segment. Aft segment free of inhibitor.
LP3 C		Mid segment inhibitor moved to segment aft end.
LP3 D		Mid and aft segment replaced by a single longer segment
LP3 E		Aft segment free of inhibitor

**Figure 6: The LP3 Configurations.**



These configurations permitted a parametric study of the second inter-segment arrangement (termed IS2) which was suspected to be at the origin of the unstable sheared flow capable of driving motor instability.

Configurations A, D and E produced the most remarkable results, with clearly different behaviors. The figures below, taken from reference [33] illustrates these results. They show head end pressure power spectral densities (psd).

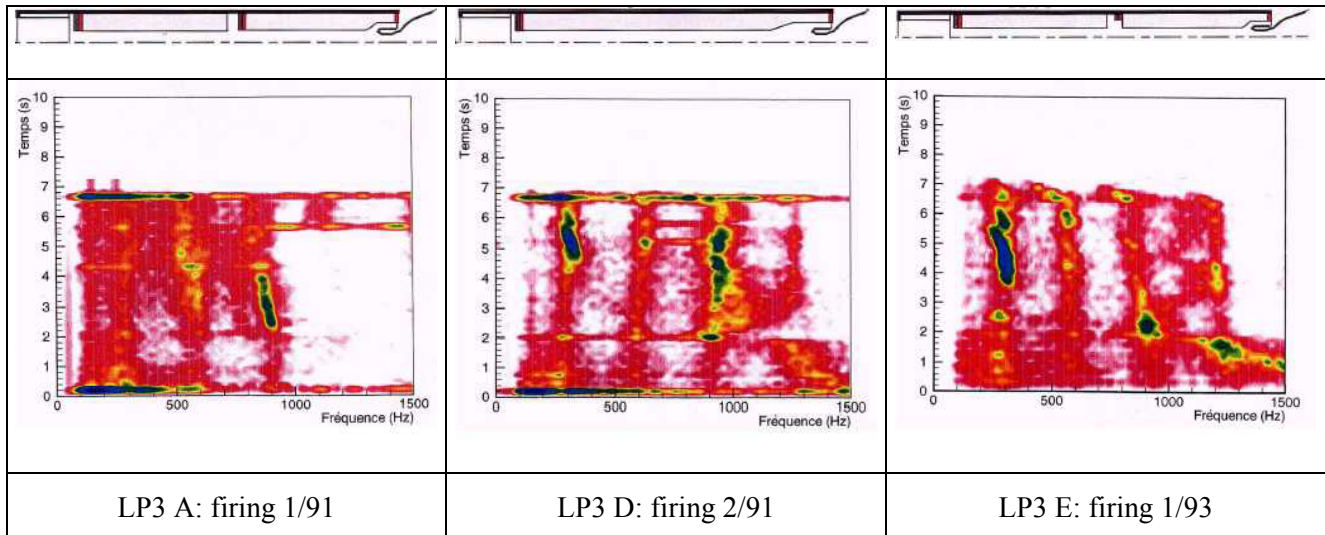


**Figure 7: Typical Results of LP3 Motors (Head-End Power Spectral Densities)**

**NB :  $f_{1L} \approx 300$  Hz,  $f_{2L} \approx 600$  Hz,  $f_{3L} \approx 900$  Hz.**

These results show that all three configurations were unstable and that the frequency tracks were organized around the first three longitudinal modes. Decreasing frequency tracks with sudden jumps are clearly visible and indicate that the observed instabilities belong to flow driven instability regimes. References [24, 25] present the results of the acoustic balance approach that was applied to all LP3 configurations and concluded that the motors should be stable. These results were at the origin of a brand new understanding of flow instabilities. Before these results, it was accepted that in segmented motors, like those of the US Space Shuttle, US Titan launcher or the European Ariane 5 MPS, the protruding inhibitor ring at the IS2 location was the major source of vortex-shedding, due to the highly sheared flow around the obstacle created by the protrusion of the inhibitor. This situation is present in LP3 A and results show that it produces instabilities, early in the burn, at high frequencies (around the third longitudinal mode, close to 900 Hz). The other results were rather surprising, since significant amplitudes were recorded despite the motor configurations do not comprise protrusion of obstacle in the flow. This was viewed as an indication that another mechanism for flow instabilities was present. The fact that LP3 D configuration was unstable was in itself like an earthquake in our understanding. How such a simple geometry (at the time where instabilities are observed, the motor was very much a pure cylindrical grain) can produce flow instabilities ? This question motivated the throughout analysis of the Taylor's flow stability, as described in the second paper. The results of that analysis were beyond all expectations. They clearly showed that the simple Taylor's flow bore in itself the roots of instabilities [34]. This rather simple flow (velocity field expresses as mere sine and cosine laws) was found to undergo intrinsic destabilization at a moderate critical abscissa of  $x/R$  close to 3 (for axisymmetric configurations), and mostly independently of the flow Reynolds number. Moreover the frequencies of the early unstable waves were found to lie in the range of longitudinal acoustic mode frequencies. This opened the way for a radically new interpretation of unstable flow regimes, driven by intrinsic flow instability. This was supported by unprecedented full numerical simulations of motor instabilities [35]. These showed that observed instabilities in LP3 D and LP3 E configurations were of a same nature and implied a coupling of

Taylor's flow intrinsic unstable waves with longitudinal acoustic modes of the chamber. This coupling produced what was called parietal vortex-shedding: vortices are generated at the burning surface and move downstream until they interact with the submerged nozzle. Afterward, it was noted that first hints of Taylor's flow instabilities were mentioned and detailed in the synthesis article of Dunlap *et al.* [36].

### Simplified Approaches

In the quest for situations that would permit the full numerical model validation it was decided to use Flandro's approach to devise the simplest motor that could produce vortex-shedding driven instabilities. From the ingredients of Flandro's explanation to unstable motor it was retained that, in order to devise a "whistling motor", one would need to produce a mean flow with a localized inflectional profile whose unstable frequencies could match the chamber first longitudinal modes frequencies. That work, described in details in [17, 23], consisted in devising an unstable motor from first principles and is worth being related here as an example of the use of simplified methods to analyze flow driven instabilities. The starting point is a simple motor geometry used for code evaluation that comprises a prismatic grain geometry. This geometry produces an inflectional velocity profile at the exit of the cylindrical portion of the grain (here  $x=155$  mm), as described in figure 8 below.

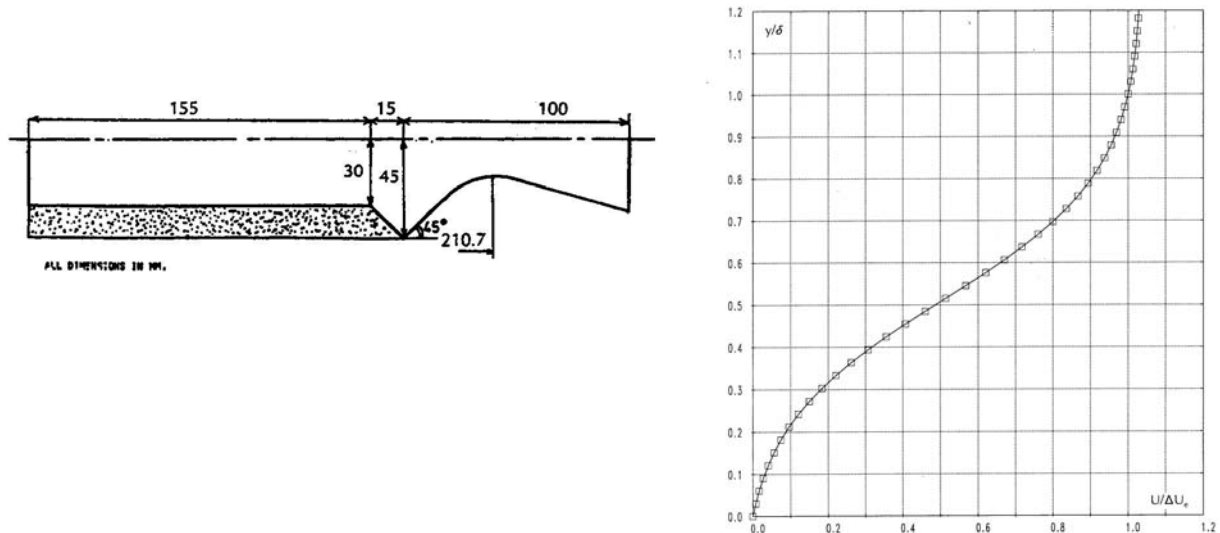


**Figure 8: Simple Motor Geometry Producing an Inflectional Velocity Profile at  $x=155$  mm.**

Under the assumption of parallel flow, it is possible to characterize the stability properties of this profile from Orr-Sommerfeld type equations, in their spatial growth formulation. In this formulation velocities are expressed relative to  $\Delta U$ , the velocity difference across the shear layer and distances are expressed relative to  $\delta$ , the thickness of the shear layer. The time scale is thus  $\delta/\Delta U$ . The main result is the complex dimensionless wave number  $a = a^r + ia^i$ , obtained as a function of the real dimensionless frequency, expressed as a Strouhal number,  $c^r = 2\pi f\delta/\Delta U$ . The opposite of the imaginary part of the wave number,  $-a^i$ , represents the spatial growth rate and the ratio  $K_v = c^r/a^r$  is the vortex phase velocity in  $\Delta U$  units. These results are depicted in figure 9 below.

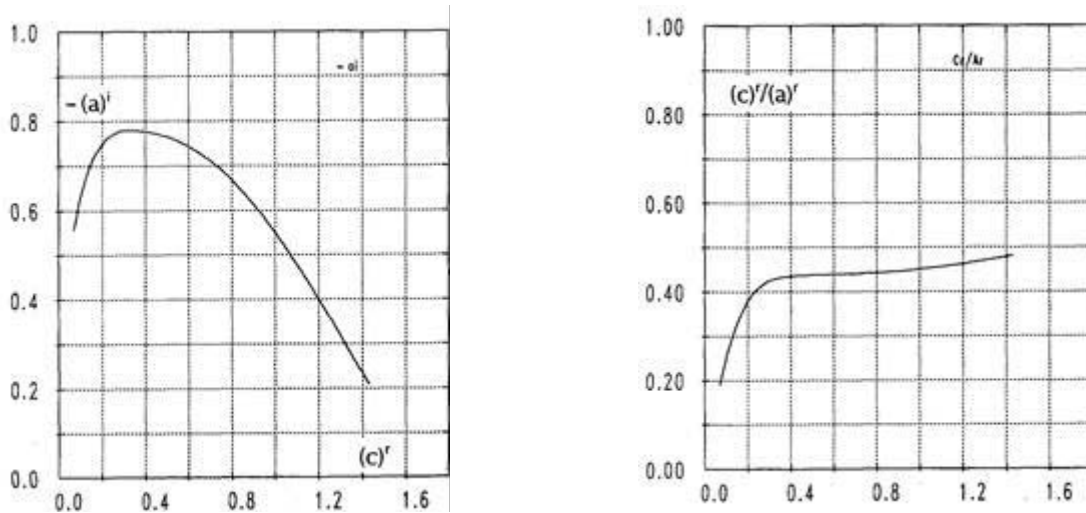


**Figure 9: Stability Properties of the Inflectional Profile.**

The results of the Orr-Sommerfeld solver can be viewed as universal curves, characterizing profiles of similar shapes, defined by their values for  $\delta$  and  $\Delta U$ . For such profiles, the most unstable frequency is given by  $c^r = 0.3$  with an associated vortical wave length,  $\lambda_v = 2\pi\delta/a^r = K_v(2\pi\delta/c^r)$ . From fig. 9 it is useful to note that there exists an upper limit ( $c^r \approx 1.6$ ) above which no unstable waves can be sustained. The coefficient  $K_v$  is the ratio  $c^r/a^r$  and is also a direct result of the velocity profile stability analysis. It represents the ratio of the vortex displacement velocity to the shear layer velocity difference  $\Delta U$ . This is a useful information if phase relationship have to be compared, as in the Rossiter's approach (coefficient  $k$ ).

In order to devise a whistling motor, one has to verify that:

- the most unstable frequency of the vortical waves matches the chamber longitudinal acoustic mode frequency,
- the stand-off distance separating the vortex emission point to the interaction point, assumed to be localized at the nozzle entrance, is sufficient to contain an integer number of vortices of wave length  $\lambda_v$ .

These two conditions are necessary conditions to produce vortex driven instabilities. Experience show that they are also, in most cases, sufficient conditions.

It is then a simple matter to adjust the motor chamber length (which governs the frequency of the  $q^{\text{th}}$  longitudinal mode,  $f_q = q a_0/2L$ ), by increasing the distance between the downstream end of the propellant grain and the nozzle, to verify the two conditions stated above. Considering an actual motor, propellant combustion implies a continuous increase of the internal grain port diameter,  $D$ , and consequently a continuous decrease of the mean flow axial velocity,  $U$ , at the grain downstream end (from simple mass balance). Assuming that  $\delta$  and  $\Delta U$  are known functions of  $D$  and  $U$ :  $\delta = K_\delta D$  and  $\Delta U = K_U U$ , one can follow the evolution of the vortical wave properties during motor burn. This will permit final adjustments. This exercise was performed on a laboratory scale motor configuration and resulted in the C1xb motor depicted in figure 10 below. The stand-off distance from propellant end to the nozzle entrance plane was adjusted to provide frequency match during most of the motor burn time. In the frequency versus propellant web distance burned plot, we followed the time evolution of the frequencies corresponding to  $c^r = 0.3$  (most amplified frequency) and  $c^r = 1.6$  (upper frequency limit of the unstable velocity profile) in the grid formed with the chamber acoustic mode frequencies (horizontal lines). It clearly appears that



## Motor Flow Instabilities – Part 1

the range of possibly excited modes rapidly narrows to the first acoustic mode, in the second half of the firing.

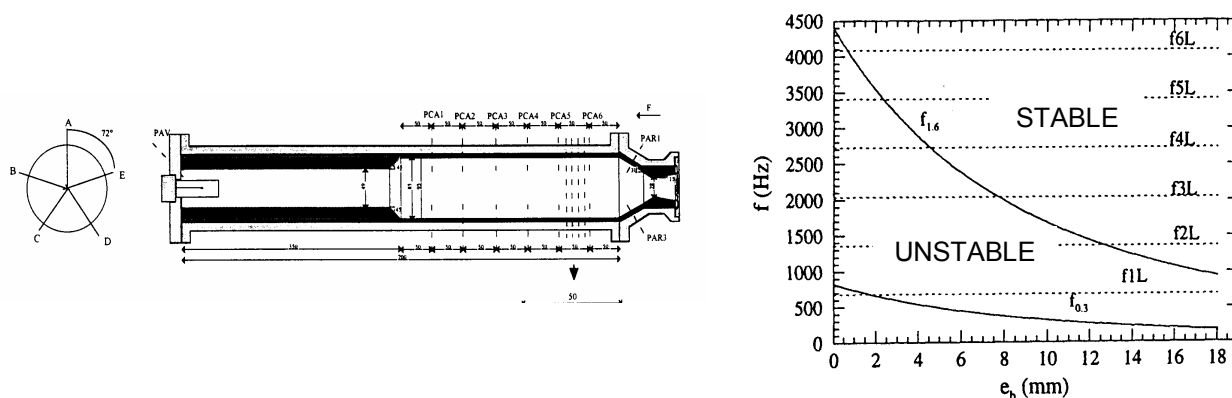


Figure 10: C1xb Motor Design from the Simple Frequency Match.

Although the acoustic frequencies never match the most amplified frequency, it was anticipated that the motor would be unstable. Indeed, a coupling path is available since the acoustic frequency of the first mode lies in the range of the shear layer unstable frequencies. In that vision, the shear layer is a mere broad band amplifier and will naturally tune to available frequencies. This actually worked. The C1xb motor was constructed and fired several times at ONERA, in the framework of J. Dupays's thesis [37, 38]. Good reproducibility was observed and the motor was used in the validation work of the full numerical approaches (see below). Figure 11 illustrates the results of one C1xb firing. It clearly shows that, after a first phase where higher frequencies are present a second phase occurs with a clear flow driven motor destabilization on the first mode frequency, around 700 Hz.

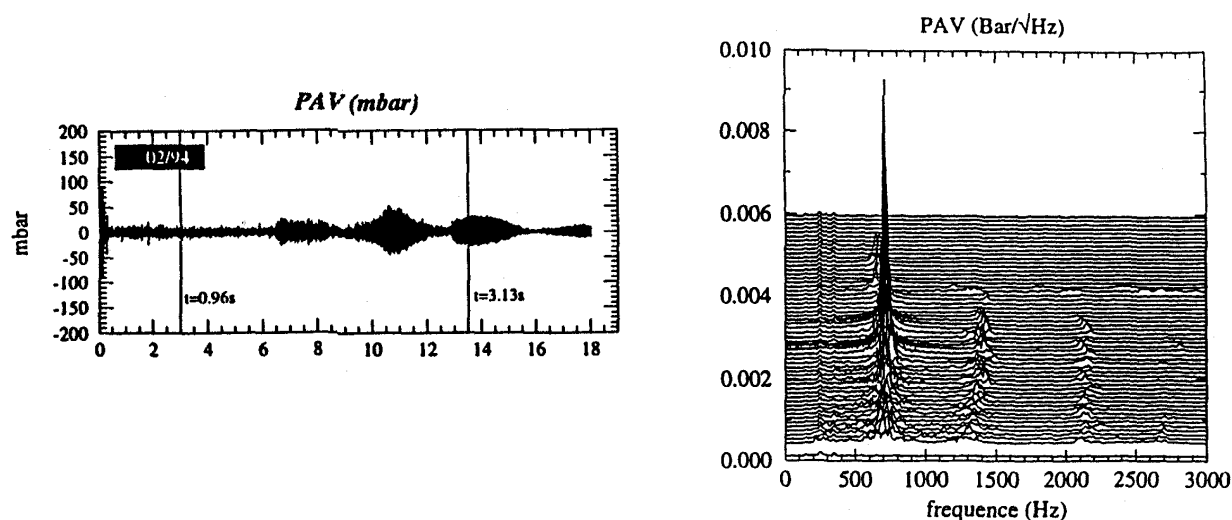
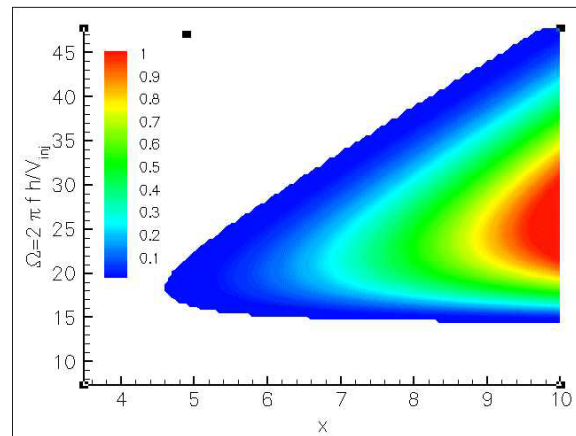


Figure 11: Example of One C1xb Firing Test. Head end unsteady pressure time history and psd.

The same simplified approach can be carried out from the stability properties of the Taylor's flow (detailed in the second part of this paper). The starting point is again the frequency range of early vortical waves. Again, the velocity and length scales are directly obtained from the stability analysis:  $V_{inj}$  is the injection velocity, and  $h$ , the height (or radius) of the chamber. The knowledge of the frequencies of possible unstable waves, in  $V_{inj}/h$  units, permits to identify configurations whose acoustic frequencies of

interest can be matched. This provides the necessary ingredients for positive coupling and permits to identify configurations that would be prone to acoustic resonances. Again this exercise was done for the 2D planar VECLA cold gas set-up and produced remarkable results [39-42]. Figure 12 below represents the results of the hydrodynamic stability analysis in the form of the wave growth factor as a function of dimensionless frequency and the dimensionless distance from the head-end.



**Figure 12: Results of the Stability Analysis of the Taylor’s Flow. Spatial amplification factor as a function of dimensionless frequency and distance from the head-end.**

However, simple frequency match considerations are not always sufficient to describe conditions for acoustic resonances, in particular for the type of instability like Taylor’s flow instability. Other parameters must be included, such as vortical wave growth distance, non-linear saturation, amplitudes, non parallel nature of the flow (its stability properties depend on  $x$ ) and phases and amplitudes at interaction points. Two critical interaction points have been identified: motor exit or nozzle entrance point where the vortices exchange energy with the acoustic waves and “receptivity” point where the acoustic waves feed back to the vortical waves. At the present time these issues are not yet fully settled, although some clear trends have been pointed out in B. Ugurtas and J. Griffond theses [43, 44].

Simple approaches are interesting because they permit to summarize the accumulated knowledge in simple relationships that help understanding the mechanisms that govern such delicate couplings. However they cannot provide quantitative results and full numerical approaches are then needed. It must be noted that although very powerful, the full numerical approaches would only give global results (much like an experiment) that will require, in turn, some form of analysis to build some knowledge.

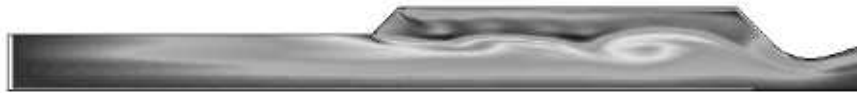
### Full Numerical Approaches

The full numerical approaches provide an unprecedented mean to analyze the details of the flow field during flow driven motor instabilities. In particular, the ability to see the internal details of the flow field has proven to be useful in classifying the flow regimes that led to motor instabilities. We already mentioned the role of the numerical simulations in pinpointing the Taylor’s flow instability origin of the instabilities in the LP3 D/E motor. The results of the full numerical approach permitted to identify three types of flows that led to motor instabilities.

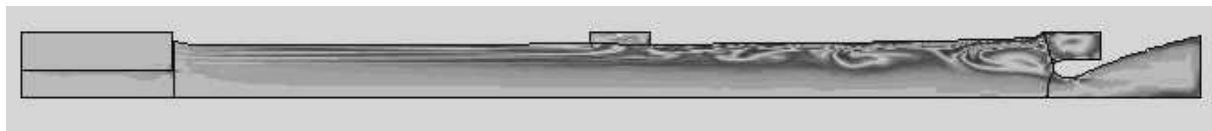
- Obstacle vortex-shedding (termed VSO from the French acronym “vortex-shedding d’obstacle”) where the shear layer responsible for the shedding of vortices is created by a protruding obstacle (such as an inhibitor ring). This corresponds to the first idea from the US experience on the Space Shuttle SRB and early Titan IIIC/D then 34D motors, but also to the nominal version of the LP3 subscale motor, LP3 A. This situation is illustrated below.



- Corner vortex-shedding (termed VSA from the French acronym “vortex-shedding d’angle”) corresponding to simplest case where shedding was produced by an obstacleless shear layer (jetting effect) corresponding to the C1xb situation, illustrated below.



- Surface or parietal vortex-shedding (VSP from the French acronym “vortex-shedding pariétal”) where the shedding results from an intrinsic instability of the internal flow, corresponding to versions D and E of the LP3 motor, without aft segment inhibitor rings, the cold flow set-up Vecla but also to the recent TITAN IV/SRMU motor. The figure below illustrates this situation.



The benefits of the full approaches are not limited to this useful insight nor to the capability to treat both acoustic and vortical waves in the single framework of the compressible full (non-linear) Navier-Stokes equations. Although important these are not sufficient to open the way to useable stability previsions in real motors. We have seen that most of the time, mild pressure oscillations are present in motors predicted stable from acoustic balance method. The important information are then the frequency and the amplitude of these pressure oscillations, as well as their efficiency in translating to thrust oscillations. The full approaches must then have the capability in providing such information. This implies that some of the phenomenons identified in fig. 1 that are missing in the approach have to be taken care of. Since phenomenons numbered 2, 3 and 5 (nozzle flow, vorticity waves and vortex-shedding) are already included in the full Navier-Stokes approach, models must be devised for including the phenomenons numbered 1, 4 and 6 on fig. 1 (propellant combustion, two-phase flow and turbulence). To these internal phenomenons, the possible coupling with the motor case or elements of structure must be added. Under these conditions, the full numerical approaches will become a useful tool for an oscillation free motor design (quiet motor).

Research work is heading in that direction and the present state of the art is coming close to that requirement. This will be illustrated by three examples in the next section. Most of these examples have been obtained in the validation stage. Indeed, as already mentioned, the validation of the numerical tools is of first importance and represent the price to pay for a reliable prevision of motor stability and/or control. References [45-50] are examples worth mentioning to complement other cited references.

## Examples

### Example 1: The C1xb and VSA

From the beginning, the C1xb motor was designed as to be a first stage of validation at the laboratory scale. As described in J. Dupays’ thesis the emphasis was put on the two-phase flow effects, combined with vortex-shedding driven oscillations. Following first demonstration of effective motor destabilization, as presented here above, the motor was fired with propellants having different inert particle loadings. Although this work produced unprecedented results, in particular on the influence of the inert particles on

oscillatory levels (to the contrary of the ideas inherited from the acoustic balance approach described earlier, amplitudes were not always decreased by the presence of condensed phase) it was limited by the difficulties in characterizing the propellant combustion response. A quantitative comparison in term of frequency and amplitude was nevertheless conducted few years later, once propellant characterization became available. This is described in [51] and the main results are presented below. The propellant response function is treated as an unsteady boundary condition that is derived from the linear relationship defining the pressure coupled response function  $R_{MP}(\omega) = \frac{\dot{m}'(\omega)/\bar{\dot{m}}}{p'(\omega)/\bar{p}}$ . Here  $\dot{m}$  is the injected mass flow rate, prime denotes unsteady components and overbar mean values. Then the resulting unsteady injected mass flow rate is expressed as a convolution integral:

$$\dot{m}(t) = \bar{\dot{m}} + \frac{\bar{\dot{m}}}{\bar{p}} \int_0^{t-t_0} R(\tau)(p(t-\tau) - \bar{p})d\tau$$

with  $R(\tau)$  being the impulse response associated to the frequency response  $R_{MP}(\omega)$ :

$$R(t) = \mathcal{TF}^{-1}[R_{MP}(\omega)]$$

This simple boundary condition proved to be quite effective and produced quasi-perfect agreement between the experimental measurements and the computations. Due to uncertainties in the propellant characterization two response curves were considered. Although these curves largely differed, the results were found to be significantly improved with both response functions. The figure below presents the unsteady flow field in the C1xb motor at the 10.7 mm web distance burned which was chosen for the comparison, and the following table summarizes the quantitative results, in terms of pressure amplitudes and frequency.

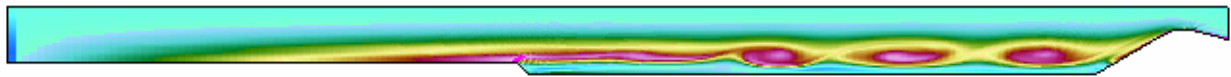


**Figure 13: C1xb Flow Field at 10.7 mm of Web Distance Burned.**

	No response	Response #1 (mne)	Response #2 (glk)	<b>Experiment</b>
Head-end amplitude (hPa) (relative error)	12.7 (71%)	28.5 (35%)	43.1 (2%)	<b>43.9</b>
Aft-end amplitude( $P_{C6}$ ) (hPa) (relative error)	15.5 (39%)	20.6 (20%)	26.6 (4%)	<b>25.6</b>
Frequency (Hz) (relative error)	740 (3.8%)	720 (1.0%)	715 (0.3%)	<b>713</b>
Frequency resolution (Hz)	23	23	23	<b>10</b>

The “no response” results were found to be improved for both response functions. In particular, the ratio of head-end to aft-end pressure amplitudes together with the oscillation frequency were found to better match the experimental measurements. Best results were obtained with the second response curve with an almost perfect agreement. It must be stressed that it was the first time that full approach results could be

compared to actual firing test measurements. The rather satisfactory agreement was seen as an evidence that the full approach was sound and could provide quantitative stability data, such as frequency and amplitude of limit cycle oscillations in actual motors.

**Example 2: The VECLA Set-Up and the VSP**

The VECLA cold flow set-up of ONERA was extensively used to understand the VSP mechanism and to validate the full numerical approach. The VECLA set-up is a modular air fed set-up. It is 2D planar and the length to height ratio can be varied through variation of chamber height (the length of the porous wall is fixed at 581 mm but the height can be varied from 30 to 10 mm). It can be tested with or without a choked nozzle. In the configuration without nozzle, the injection velocity can be easily varied by changing the air mass flow rate. This provided a very convenient mean to control the flow field inside the VECLA set-up.

At least three different behaviors were documented:

- a) For large length to height ratio ( $h=10\text{mm}$ ) transition to turbulence was observed inside the chamber.
- b) For moderate length to height ratio ( $h=20\text{mm}$ ) acoustic resonance could be produced for a definite range of injection velocity.
- c) For small length to height ratio ( $h=30\text{mm}$ ) no acoustic resonance nor turbulent transition are observed. However, the flow exhibits local instabilities that can be compared to the stability analysis.

All three regimes were used to validate the full numerical approach.

Case a) served to validate turbulence models [52] and will not be detailed here.

Case c) provided unprecedented check of the linear stability results, as described in the second paper. Unstable wave frequency range and spatial growth rate were found to match the stability results. These results were also used to check the full Navier-Stokes approach, as described in B. Ugurtas' thesis [43]. The claim was that the full Navier-Stokes solution contains the early hydrodynamically unstable waves. This was verified in case c). Simulations were performed and the unsteady field was extracted from the full Navier-Stokes solutions by Fourier transforms at given frequencies. The shape and growth rate of the unstable waves were compared to the linear stability results and showed good agreement, as illustrated by the figures 14 and 15 below.

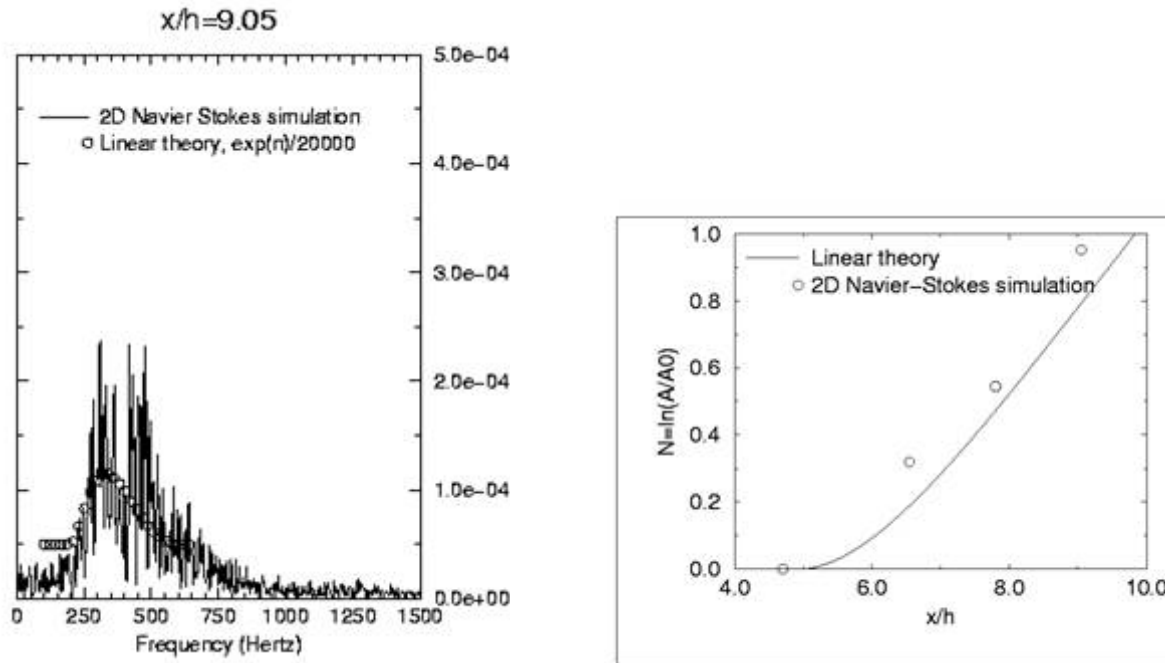


Figure 14: Comparison of the Navier-Stokes Results with the Linear Stability Analysis.  
Velocity spectrum and spatial amplification factor.

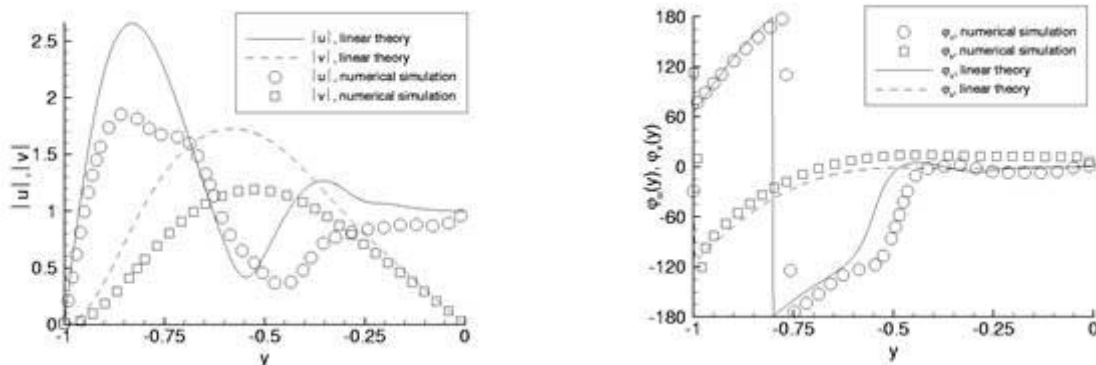
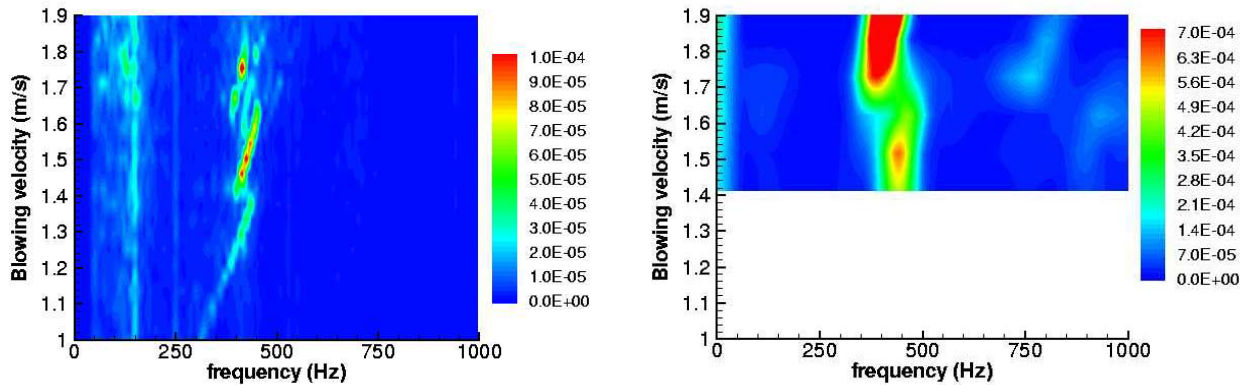


Figure 15: Comparison of the Navier-Stokes Results with the Linear Stability Analysis.  
Amplitude and phase of the velocity radial profile.

This established the ability of the Navier-Stokes solver to properly describe the early destabilization processes of the Taylor's flow.

Case b) was also used to check the ability of the full Navier-Stokes approach to reproduce acoustic resonance regimes. For this case, the ratio  $V_{inj}/h$  could be adjusted so as the unstable stability wave frequencies match the chamber longitudinal mode frequencies. Clear cases of acoustic resonance could be observed in a definite injection velocity range. By imposing a time variation of the injection velocity in the Navier-Stokes simulations resonances could be simulated in good agreement with the experimental results. This is illustrated by figure 16 below.





**Figure 16: Comparison of the Navier-Stokes Results (right) with the Experimental Results (left). Velocity psd as a function of the injection velocity.**

Satisfactory qualitative agreement is observed, establishing the ability of the full approach to reproduce resonant regimes in VSP situations. However, the oscillatory amplitudes were found to be over-estimated. Reference [53] presents an effort to bridge the amplitude gap. In that work, the negative response function of the porous wall was included in the simulation (on the contrary to burning propellant, the porous wall has a negative response to pressure waves, resulting in significant damping of the excited acoustic waves). In an attempt to better stick to the experiment, the flow destabilization in the numerical solution relied on a white noise, introduced at the porous surface vicinity, whose characteristic was matched with the measured injection noise. This produced a marked decrease of the simulated oscillatory amplitude being now comparable to actually measured amplitudes, as displayed in figure 17.

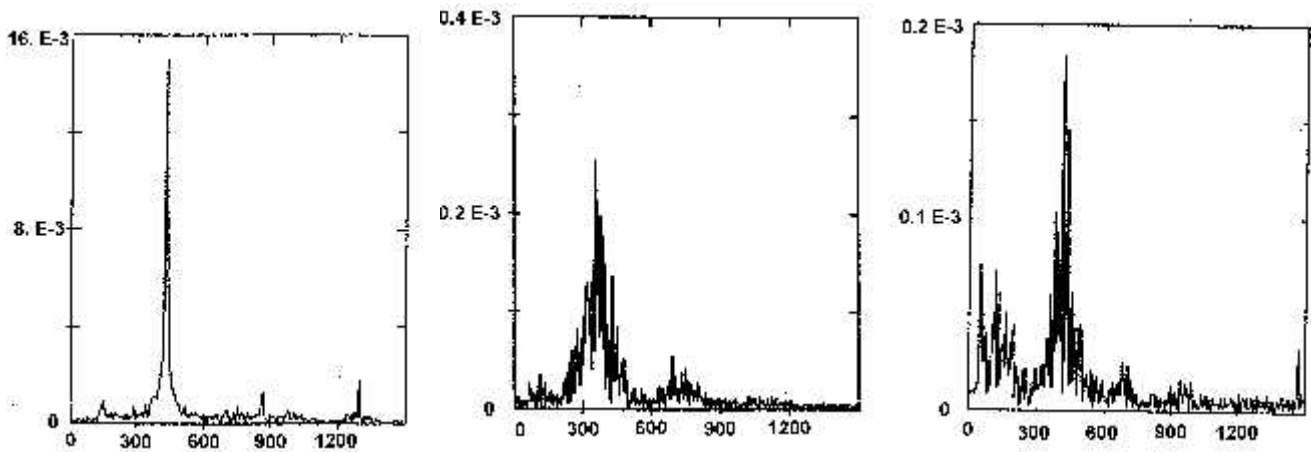


**Figure 17: Head-End Pressure Spectra. From left to right: a) Initial Navier-Stokes solution; b) Navier-Stokes with porous wall response and white noise model; c) Experiment.**

The exemplary simplicity of the VECLA set-up permitted to go one step further in establishing the validity of the full numerical approach and to actually see the so-called parietal vortices. Following Prof. Culick's suggestion, the injected flow was seeded with acetone and laser induced fluorescence permitted to actually see the vortices in the VECLA set-up [54]. It must be stressed that this constituted a world premiere that confirmed that the computed vortices were indeed present in the experimental set-up. Figure 18 below illustrates this result.

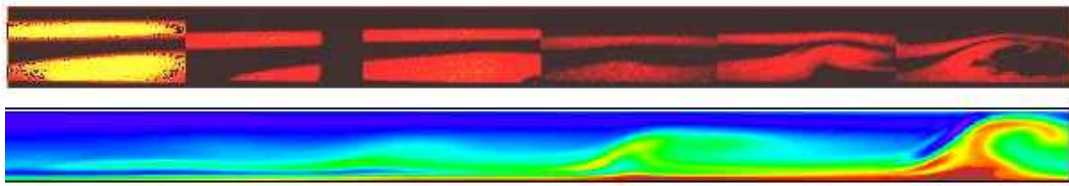


**Figure 18: PLIF Images of Vortices in VECLA Set-Up (top)  
Compared to the Computed Vorticity Field (bottom).**

### Example 3: An Actual Motor (VSP + VSO)

Application to an actual full scale motor was rendered possible by the validation effort depicted in the preceding examples and completed by a two-phase flow model that was also validated [37-38, 55]. Considering that the actual Ariane 5 motor used an aluminized propellant, the two-phase flow solver was completed by a very basic aluminum combustion model. This model was based on the  $d^2$  model that links the aluminum droplet burn time to the square of its diameter. Realistic value for the reaction heat was used. The inter-phase source terms in the balance equations were thus modified to include the mass and energy exchanges due to droplet combustion. This is detailed in reference [56].

Then the early K4 configuration of the Ariane 5 P230 was simulated, with or without the reactive two-phase model. The chosen time point was that of maximum of observed oscillatory amplitude. The retained experimental configuration was that of the M1 firing test at 95 s into the burn.

This work showed that simulations without aluminum combustion were not satisfactory since they could not reproduce the oscillation frequency and amplitude. Detailed analysis of the numerical results showed two competing mechanisms: the VSO vortices from the protruding inhibitor, at a higher frequency, close to the third acoustic mode frequency and the VSP vortices that developed along the aft segment, at the lower first mode frequency. This competition resulted in the absence of acoustic resonance. On the other hand, when aluminum combustion was introduced, the VSP was reinforced to the point that it became dominant and forced the VSO to tune to the first acoustic mode frequency. This resulted in marked resonance in better agreement with the experimental results. This is illustrated by the following figure.

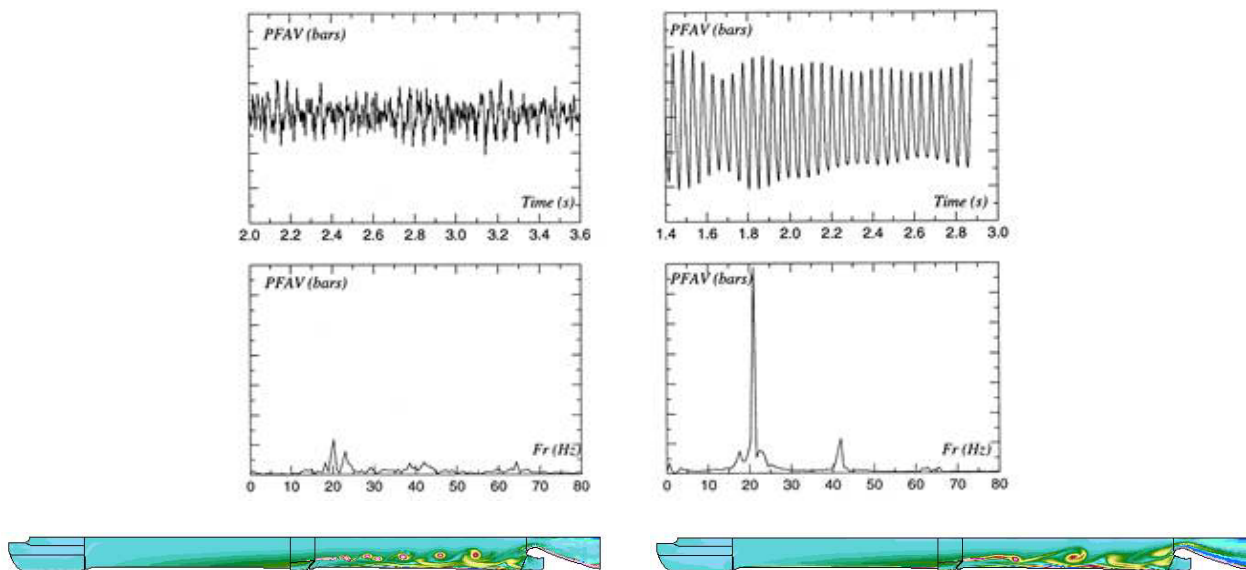


**Figure 19: M1 Results for the Single Phase (left) and Reactive Two-Phase (right) Models.  
Head-end pressure time history and spectrum, vorticity field.**



The computed frequency was then close to the first acoustic mode frequency and the oscillatory amplitudes were comparable to the measured amplitudes. Of course, this result depends on the model inputs, particularly the size of the aluminum droplets and of the alumina residues, as well as on model details or inhibitor ring properties (deformation, vibrations, ...) which may have some incidences on the computed flow field. Such data are still not perfectly known and some characterization and modeling works are still needed before a satisfactory prediction can be guaranteed in such complex full scale motor configurations.

### Example 4: Active Control Demonstration

To complete this example section, it is interesting to illustrate the capability of the full numerical approach to validate closed loop active control concepts. The idea was to use the full Navier-Stokes solution to evaluate control strategies and to demonstrate the feasibility to control flow driven instabilities. It was then decided to use the simulated flow field in the simplest VSA configuration. The test case C1 was used. This test case is the first configuration designed with the simplified approach, as described above for the C1xb motor. On the contrary to the C1xb motor, it is a purely numerical test case [23] that has been used at the beginning of the Navier-Stokes codes validation effort. It is fully documented and has been computed many times by many codes.

Roughly speaking, the active control loop is composed of:

- A transducer that records the state of the internal flow,
- An actuator that is capable of acting on the flow field,
- A controller that processes the transducer signal into a signal that is fed to the actuator.

This is completed by an identification step that defines the actual transfer function between the actuator and the transducer.

During operation, the controller adjusts its own transfer function to minimize the output signal of the transducer.

The work presented here is the result of a cooperation between the EM2C lab at ECP and ONERA. It is described in details in M. Mettenleiter's thesis and in reference [57, 58].

Transducer was normally taken as computed pressure at the nozzle entrance section but a numerical vorticity transducer was also tested. Actuator was modeled by distributed mass sources, representing an injection of a reactive fluid. Actuator was placed at the chamber head-end (case 1) but some tests were also performed with an actuator placed in the vicinity of the unstable shear layer (case 2). Figure 20 below presents the control scheme for C1 test case. Two main control strategies were tested. They belonged to anti-noise control and to noise source control. In the latter strategy the aim is to actively control the source at the origin of the acoustic resonance rather than controlling the resulting acoustic wave.

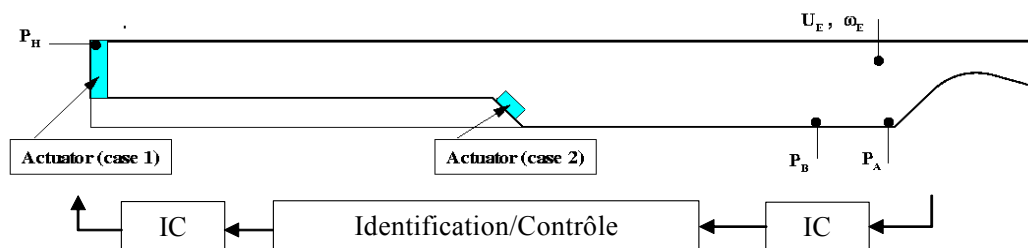
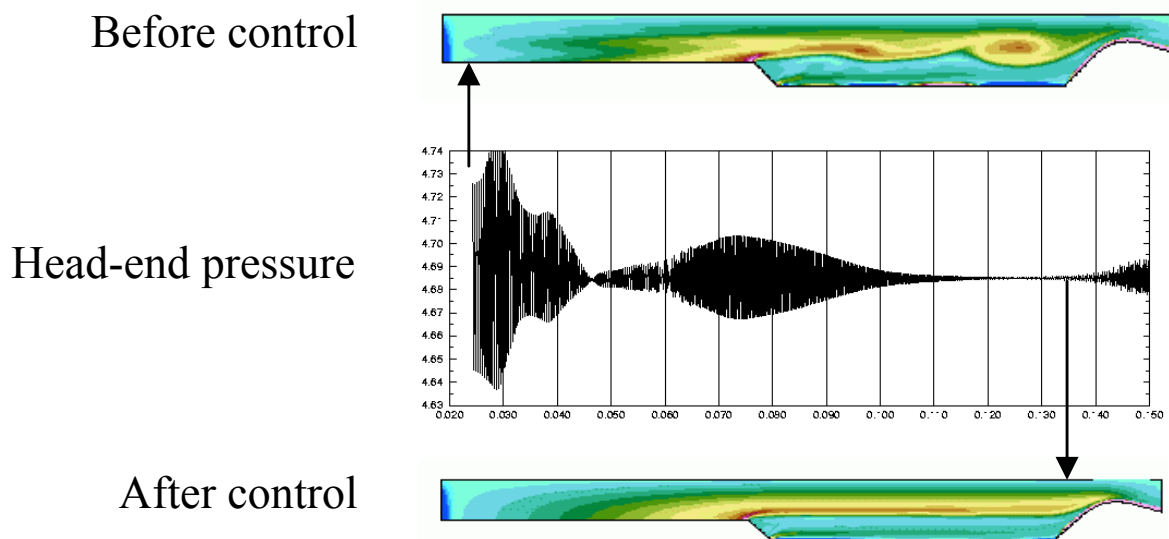


Figure 20: Control Schemes for the C1 Test Case.

The control algorithm was introduced as Fortran subroutines into the Navier-Stokes solver. Special attention was given to the calling sequence between the Navier-Stokes solver iterative time integration and the controller own process. Adapted filtering steps were added to the coupling procedure, in order to take care of the very different time scales between the two programs. Indeed, the time step of the explicit Navier-Stokes solver is of the order of  $10^{-7}$  s, while the time scale of the controller is of the order of  $10^{-4}$  s. Under such conditions, very significant reductions of the oscillatory amplitude could be demonstrated. One of the difficulty was that the acoustic resonance could occur in a large frequency range. This is illustrated on figure 10 that shows that at given web distance burned, several acoustic modes lie in the unstable range. The direct consequence was that once the motor was controlled on its initial resonant frequency, it shifted to another resonance at a higher frequency, corresponding to the next acoustic mode. Then the controller had to adjust itself to the new condition. This illustrated the benefit of an adaptive active control loop, as the one proposed by EM2C/ECP, for the flow driven instability under consideration.

Control was achieved in the standard configuration (nozzle end pressure transducer + head-end actuator) that could correspond to an actual motor configuration. However, the numerical approach permitted to test other configurations, not yet fully adaptable to an actual motor, such as the vorticity transducer combined with an actuator located in the vicinity of the unstable shear layer (case 2). Not surprisingly, this latter configuration exhibited better performance in term of time to control and residual amplitudes. Figure 21 below illustrates this performance.



**Figure 21: Demonstration of Adaptive Active Control in C1 Test Case (Case 2).**

## CONCLUSIONS/UNSETTLED ISSUES

The intensive research effort conducted in the past 12 years in the framework of the European Ariane 5 launcher related programs has produced a new vision for motor instability. It is now clear that instabilities must be approached in a global fashion that puts the internal flow field and related phenomenons, such as gaseous and condensed phase combustion, vorticity (in the form of acoustically forced vorticity waves, developed vortices or early flow instability waves) and structural response, in the center of the investigation. The early acoustic balance approaches, although extremely profitable in term of understanding and isolating physical phenomenons, could not produce the expected answers for motor sustaining mild amplitude limit cycle pressure oscillations.

It has been shown that under the condition that the necessary validation and characterization efforts were conducted, the numerical solution to the full unsteady compressible Navier-Stokes equations, together with ad hoc models for coupled mechanisms, could produce valuable results in close agreement with experimental measurements.

Of course obtaining meaningful numerical solutions, in particular in such a challenging and delicate context remains a difficult task. The grid issue is undoubtedly one of the most crucial issue. In order to stay within acceptable limits in terms of computer CPU time and memory occupation, the grid must be tailored to each case. Our ability to produce adequate grids is then a direct function of our knowledge of what the important flow features are and where they are located. This clearly limits the use of the full numerical approach to documented situations and a priori predictions cannot be guaranteed in any situation. However, once the applicability has been established for a given type of configurations, the numerical approach can be used with large benefits to analyse and optimise the configuration.

Another limitation is the choice of the proper models to describe non flow related mechanisms such as combustion, structural response, ... These models bear their own limitations that are of two types: the physics that is included in the models and the necessary inputs to the models. Both limitations can impair the successful application of the model into the numerical solution. Aluminum combustion is presently one area where progresses are expected for both types of limitations. This implies dedicated experiments and analyses to better describe the complex mechanisms that govern the formation of aluminum droplets, their combustion and finally the production of alumina droplets in complex flow fields. In particular the question of droplet interactions in a large population of various sizes and compositions, remains open.

Finally, several years of experience with full numerical solutions, where most often several models are coupled in a non-linear fashion, have put to light many unexpected or surprising results. It is always surprising to realize that the resulting behavior is not the mere addition of individual effects or that a linearly damping mechanism can increase the limit cycle amplitude. This departure from the common linear thinking poses some problems when results are to be analyzed, understood and finally validated or accepted. This difficulty, far from being a mere curiosity, renders the progressive validation approach mandatory, in order to know how confident one can be when confronted to unexpected results. Often, the simplified approaches can be called in to help analyzing the results.

Most often success lies in a proper combination of both approaches. It is then recommended that the rocket engineer who has to deal with instabilities exercise in both approaches.

## **ACKNOWLEDGEMENT**

The authors want to acknowledge supports from BPD, CNES and ONERA that permitted to carry out some of the research activities mentioned in this talk. They are also indebted to all their colleagues at ONERA, with particular attention to P. Kuentzmann, for his continuous encouragements, N. Lupoglazoff, for his essential contribution to the numerical simulations, G. Avalon, J. Dupays, M. Prevost, J.-C. Traineau, Y. Fabignon, C. Caugant (now retired) for many fruitful and unlimited discussions.

## **REFERENCES**

- [1] Kuentzmann P., "Combustion Instabilities," AGARD LS-180, September 1991.
- [2] Culick F.E.C. and Yang V., "Prediction of the Stability of Unsteady Motions in Solid Propellant Rocket Motors," Nonsteady Burning and Combustion Instability of Solid Propellants, Vol. 143, Progress in Astronautics and Aeronautics, Edited by L. De Luca, E.W. Price, and M. Summerfield, AIAA, New York, 1992, pp. 719-779.

- [3] Hart R.W. and McClure F.T., “Theory of Acoustic Instability in Solid Propellant Rocket Combustion”, 10th Symposium (international) on Combustion, pp. 1047-1065, 1965, The Combustion Institute, 1965, Pittsburgh PA.
- [4] Culick F.E.C., “Acoustic Oscillations in Solid Propellant Rocket Chambers”, *Astronautica Acta*, Vol. 12, No. 2, 1966, pp. 113-125.
- [5] Culick F.E.C., “The Stability of One Dimensional Motions in a Rocket Motor”, *Combustion Science and Technology*, 1973, Vol. 7, pp. 165-175.
- [6] Culick F.E.C., “The Stability of Three Dimensional Motions in a Combustion Chamber”, *Combustion Science and Technology*, 1975, Vol. 10, pp. 109-124.
- [7] Vuillot F., “Acoustic Mode Determination in Solid Rocket Motor Stability Analysis”, *J. of Propulsion and Power*, Vol. 3, No. 4, July-August 1987.
- [8] Flandro G.A., “Solid Propellant Acoustic Admittance Corrections,” *Journal of Sound and Vibration*, Vol. 36, No. 3, 1974, pp. 297-312.
- [9] Vuillot F. and Avalon G., “Acoustic Boundary Layers in Solid Propellant Rocket Motors Using Navier-Stokes Equations”, *J. Propulsion and Power*, Vol. 7, No. 2, March-April 1991, pp. 231-239.
- [10] Flandro G.A., “Effects of Vorticity on Rocket Combustion Stability”, *J. of Propulsion and Power*, Vol. 11, No. 4, July-August 1995, pp. 607-625.
- [11] Vuillot F., “Numerical Computation of Acoustic Boundary Layers in Large Solid Propellant Space Booster”, AIAA 91-0206, AIAA 29th Aerospace Sciences Meeting, Reno, Nevada, USA, January 1991.
- [12] Vuillot F. and Kuentzmann P., “Flow Turning and Admittance Corrections: An Experimental Comparison”, *J. of Propulsion and Power*, Vol. 2, No. 4, July-August 1986, pp. 345-353.
- [13] Van Moorhem W., “Flow Turning in Solid Propellant Rocket Combustion Stability Analyses”, *AIAA Journal*, Vol. 20, No. 10, pp. 1420-1425, October 1982.
- [14] Majdalani J. and Van Moorhem W.K., “Laminar Cold-Flow Model for the Internal Gas Dynamics of a Slab Rocket Motor”, *Aerosp. Sci. Technol.* 5 (2001) 193-207.
- [15] Temkin S. and Dobbins R.A., “Attenuation and Dispersion of Sound by Particulate-Relaxation Processes”, *J. of Acoustical Society of America*, Vol. 40, No. 2, 1966.
- [16] Flandro G.A. and Jacobs H.R., “Vortex Generated Sound in Cavities”, AIAA Paper 73 1014, Seattle, Washington, USA, October 1973.
- [17] Vuillot F., “Vortex-Shedding Phenomena in Solid Rocket Motors”, *Journal of Propulsion and Power*, Vol. 11, No. 4, pp. 626-639, July-August 1995.
- [18] Dunlap R. and Brown R.S., “Exploratory Experiments on Acoustic Oscillations Driven by Periodic Vortex Shedding”, *AIAA J.*, Vol. 19, No. 3, 1981.
- [19] Brown R.S., Dunlap R., Young S.W. and Waugh R.C., “Vortex Shedding as a Source of Acoustic Energy in Segmented Solid Rockets”, *J. of Spacecraft and Rocket*, Vol. 18, No. 4, pp. 312-319, July-August 1981.

## Motor Flow Instabilities – Part 1

---

- [20] Dotson K.W., Koshigoe S. and Pace K.K., “Vortex Shedding in a Large Solid Rocket Motor Without Inhibitors at the Segment Interfaces”, J. of Propulsion and Power, Vol. 13, No. 2, March-April 1997, pp. 197-206.
- [21] Flatau A. and Van Moorhem W., “Prediction of Vortex Shedding Responses in Segmented Solid Rocket Motors”, AIAA-90-2073, AIAA 26th Joint Propulsion Conference, July 1990, Orlando, USA.
- [22] Flandro G.A., “Vortex Driving Mechanism in Oscillatory Rocket Flows”, Journal of Propulsion and Power, Vol. 2, No. 3, pp. 206-214, May-June 1986.
- [23] Lupoglazoff N. and Vuillot F., “Numerical Simulation of Vortex Shedding Phenomenon in 2D Test Case Solid Rocket Motors,” AIAA 92-0776, AIAA 30th Aerospace Sciences Meeting, Reno, Nevada, USA, January 1992.
- [24] Vuillot F., Traineau J.C., Prevost M. and Lupoglazoff N., “Experimental Validation of Stability Assessment Methods for Segmented Solid Propellant Motors”, AIAA 93-1883, AIAA 29th Joint Propulsion Conference, June 1993, Monterey, CA.
- [25] Vuillot F., “Prise en compte du détachement tourbillonnaire dans les approches linéarisées par la méthode de Flandro”, Colloque CNES-ONERA “Fonctionnement des Moteurs à Propergol Solide Segmentés pour Lanceurs Spatiaux”, 8-9 decembre 1992, Châtillon, FRANCE.
- [26] Brown R.S., Blackner A.M., Willoughby P. and Dunlap R., “Coupling Between Velocity Oscillations and Solid Propellant Combustion,” AIAA Paper 86 0531 AIAA 24th Aerospace Sciences Meeting, January 1986, Reno, Nevada.
- [27] Mason D.R., Folkman S.L. and Behring M.A., “Thrust Oscillations of the Space Shuttle Solid Rocket Booster Motor During Static Tests”, AIAA Paper 79 1138, AIAA 15th Joint Propulsion Conference, Las Vegas, June 18-20, 1979.
- [28] Mathes H.B., “Assessment of Chamber Pressure Oscillations in the Shuttle Solid Rocket Booster Motors”, AIAA paper 80 1091, AIAA 16th Joint Propulsion Conference, Hartford CT, June 1980.
- [29] Alden R.J., “Improved Performance 3.05 m (120 in.) Boosters for the Air Force Titan 34D Space Launch Vehicle,” The 1983 JANNAF Propulsion Meeting, Vol. 1, pp. 15-27; 83N 35012.
- [30] Blomshield F. and Mathes H.B., “Pressure Oscillations in Post Challenger Space Shuttle Redesigned Solid Rocket Motors”, J. of Propulsion and Power, Vol. 9, No. 2, March-April 1993, pp. 217-221.
- [31] Scippa S., Pascal Ph. and Zanier F., “Ariane 5 MPS Chamber Pressure Oscillations Full Scale Firings Results Analysis and Further Studies”, AIAA paper 94-3068, 30th AIAA Joint Propulsion conference, June 27-29, 1994, Indianapolis, IN, USA.
- [32] Prevost M., Vuillot F. and Traineau J.C., “Vortex-Shedding Driven Oscillations in Subscale Motors for the Ariane 5 MPS Solid Rocket Motors”, AIAA96-3247, 32nd AIAA Joint Propulsion Conference, Orlando, USA, July 1-3, 1996.
- [33] Prevost M., Dommée Y. and Maunoury J., “Programme POP, synthèse de la base de données expérimentales instationnaires (révision 5)”, ONERA RT 4/05212 DMAE, juin 2001.

- [34] Vuillot F., Casalis G., Avalon G. and Lupoglazoff N., “Mise en résonance acoustique d’une cavité par l’instabilité naturelle d’un écoulement généré par injection pariétale”, CR Acad. Sci. Paris, t. 327, Série II b, p. 77-83, 1999.
- [35] Lupoglazoff N. and Vuillot F., “Parietal Vortex Shedding as a Cause of Instability for Long Solid Propellant Motors. Numerical Simulations and Comparisons with Firing Tests”, AIAA 96 0761, AIAA 34th Aerospace Sciences Meeting, Reno, Nevada, USA, January 1996.
- [36] Dunlap R., Blackner A.M., Waugh R.C., Brown R.S. and Willoughby P., “Internal Flow Field Studies in a Simulated Cylindrical Port Rocket Chamber,” J. of Propulsion and Power, Vol. 6, No. 6, November-December 1990, pp. 690-704.
- [37] Dupays J., “Contribution à l’étude du rôle de la phase condensée dans la stabilité d’un MPS pour lanceur spatial”, Thesis dissertation, INPT, novembre 1996.
- [38] Dupays J., Prevost M., Tarrin P. and Vuillot F., “Effects of Particulate Phase on Vortex Shedding Driven Oscillations in Solid Rocket Motors”, AIAA 96-3248, AIAA 32nd Joint Propulsion Conference, July 1-3 1996, Orlando, USA.
- [39] Avalon G., Casalis G. and Griffond J., “Flow Instabilities and Acoustic Resonance of Channels with Wall Injection,” AIAA paper 98-3218, AIAA 34th JPC, Cleveland, July 13-15, 1998.
- [40] Casalis G., Avalon G. and Pineau J.-Ph., “Spatial Instability of Planar Channel Flow with Fluid Injection through Porous Walls”, Phys. Fluids, 10 (10), October 1998.
- [41] Ugurtas B., Avalon G., Lupoglazoff N. and Vuillot F., “Numerical Computations of Hydrodynamic Instabilities Inside Channels with Wall Injection”, AIAA 99-2505, 35th AIAA-/ASME/SAE/ASEE Joint Propulsion Conference, 20-24 June 1999, Los Angeles, CA, USA.
- [42] Ugurtas B., Avalon G., Lupoglazoff N., Vuillot F. and Casalis G., “Stability and Acoustic Resonance of Internal Flows Generated by Side Injection”, in AIAA Progress in Astronautics and Aeronautics, Volume 185, Solid Propellant Chemistry, Combustion, and Motor Interior Ballistics, Vigor Yang, Thomas B. Brill, Wu-Zhen Ren Editors.
- [43] Ugurtas B., “Etudes numérique et expérimentale des instabilités hydrodynamiques et du couplage aéro-acoustique dans un écoulement de Taylor”, Thesis dissertation, Paris 6, décembre 2000.
- [44] Griffond J., “Instabilité pariétale et accrochage aéroacoustique dans les conduits à parois débitantes simulant les moteurs à propergol solide d’Ariane 5”, Thesis dissertation, ENSAE, septembre 2001.
- [45] Lupoglazoff N. and Vuillot F., “Simulation numérique bidimensionnelle des écoulements instationnaires dans les propulseurs à propergol solide”, La Recherche Aérospatiale, No.1992-2, pp. 21-41.
- [46] Tissier P.Y., Godfroy F. and Jacquemin P., “Simulation of Three Dimensional Flows Inside Solid Propellant Rocket Motors Using a Second Order Finite Volume Method – Application to the Study of Unstable Phenomena”, AIAA 92-3275, AIAA 28th Joint Propulsion Conference, July 1992, Nashville, USA.
- [47] Lupoglazoff N. and Vuillot F., “Comparison between Firing Tests and Numerical Simulation of Vortex Shedding in a 2D Test Solid Motor” AIAA 93-3066, AIAA 24th Fluid Dynamics Conf., Orlando, FL, July 6-9, 1993.



- [48] Godfroy F. and Tissier P.Y., “CFD Analysis of Vortex Shedding Inside a Subscale Segmented Motor”, AIAA 94-2781, AIAA 30th Joint Propulsion Conference, June 1994, Indianapolis, IN.
- [49] Morfouace V. and Tissier P.Y., “Two-Phase Flow Analysis of Instabilities Driven by Vortex Shedding in Solid Rocket Motors”, AIAA 95-2733, 31st Joint Propulsion Conference July 10-12, 1995, San Diego.
- [50] Vuillot F. and Lupoglazoff N., “Combustion and Turbulent Flow Effects in 2D Unsteady Navier-Stokes Simulations of Oscillatory Rocket Motors”, AIAA 96 0884, AIAA 34th Aerospace Sciences Meeting, Reno, Nevada, USA, January 1996.
- [51] Lupoglazoff N. and Vuillot F., “Simulations of Solid Propellant Rocket Motors Instability Including Propellant Combustion Response”, 6th International Congress on Sound and Vibration, 5-8 July 1999, Lingby, Denmark.
- [52] Chaouat B., “Numerical Predictions of Channel Flows with Fluid Injection Using Reynolds Stress Model”, J. of Propulsion and Power, Vol. 18, No. 2, March-April 2002, pp. 295-303.
- [53] Lupoglazoff N. and Vuillot F., “Numerical Simulations of Parietal Vortex-Shedding Phenomenon in A Cold Flow Set-Up”, AIAA 98-3220, 34th AIAA/ASME/SAE/ASEE Joint Propulsion Conference, July 13-15 1998, Cleveland, USA.
- [54] Avalon G., Ugurtas B., Grisch F. and Bresson A., “Numerical Computations and Visualization Tests of the Flow Inside a Cold Gas Simulation with Characterization of a Parietal Vortex Shedding”, AIAA 2000-3387, 36th AIAA/ASME/SAE/ASEE Joint Propulsion Conference and Exhibit, Huntsville, AL, 16-19 July 2000.
- [55] Vuillot F., Basset T., Dupays J., Daniel E. and Lupoglazoff N., “2D Navier-Stokes Stability Computation for Solid Rocket Motors: Rotational, Combustion and Two-Phase Flow Effects”, AIAA 97-3326, 33rd AIAA/ASME/SAE/ASEE Joint Propulsion Conference, July 6-9 1997, Seattle, USA.
- [56] Lupoglazoff N., Vuillot F., Dupays J. and Fabignon Y., “Numerical Simulations of the Unsteady Flow Inside Segmented Solid-Propellant Motors with Burning Aluminum Particles”, AIAA Paper 2002-0784, AIAA 40th Aerospace Sciences Meeting, Reno, Nevada, USA, January 2002.
- [57] Mettenleiter M., “Contrôle adaptatif des instabilités aéroacoustiques. Application aux systèmes de propulsion”, Thesis dissertation, Ecole Centrale Paris, 2000.
- [58] Mettenleiter M., Vuillot F. and Candel S., “Numerical Simulation of Adaptive Control Application to Unstable Solid Rocket Motors”, Symposium RTO, Applied Vehicle Technology Panel, on Active Control Technology, 8-11 May 2000, Braunschweig (Germany), accepted for publication in AIAA Journal, 2002.